

RESTRICTED

RM A50A04a

~~1111.3~~

NACA 0005/1



NACA

RESEARCH MEMORANDUM

CHORDWISE AND SPANWISE LOADINGS MEASURED AT LOW
SPEEDS ON A LARGE TRIANGULAR WING HAVING
AN ASPECT RATIO OF 2 AND A THIN,
SUBSONIC-TYPE AIRFOIL SECTION

By David Graham

Ames Aeronautical Laboratory
Moffett Field, Calif.

CLASSIFICATION CANCELLED

Authority

D W Crawley
EO 105011

Date

12-11-53

By

DH - 1-12-54
RF - 1838

See

CLASSIFIED DOCUMENT

This document contains classified information affecting the National Defense of the United States within the meaning of the Espionage Act, USC 50:31 and 32. Its transmission or the revelation of its contents in any manner to an unauthorized person is prohibited by law. Information so classified may be imparted only to persons in the military and naval services of the United States, appropriate civilian officers and employees of the Federal Government who have a legitimate interest therein, and to United States citizens of known loyalty and discretion who of necessity must be informed thereof.

NATIONAL ADVISORY COMMITTEE
FOR AERONAUTICS

WASHINGTON
March 13, 1950

RESTRICTED

RESTRICTED

NACA RM A50A04a

[REDACTED] UNCLASSIFIED

NATIONAL ADVISORY COMMITTEE FOR AERONAUTICS

RESEARCH MEMORANDUMCHORDWISE AND SPANWISE LOADINGS MEASURED AT LOW
SPEEDS ON A LARGE TRIANGULAR WING HAVING
AN ASPECT RATIO OF 2 AND A THIN,
SUBSONIC-TYPE AIRFOIL SECTION

By David Graham

SUMMARY

Pressure-distribution and force data were measured at various angles of attack of a triangular wing of aspect ratio 2 and having an NACA 0005 modified section. The wing had a plain, constant-chord, trailing-edge flap which was deflected 0° and $\pm 10^\circ$. For the tests the Reynolds number was 15.3×10^6 and the Mach number was 0.13.

The results showed that the flow patterns and the characteristics of the wing were very similar to those presented in NACA RM A9B17, 1949, for a wing having the same plan form but a modified double-wedge section (rounded leading-edge and maximum-thickness ridges). The only significant difference was the angle of attack or lift coefficient at which the characteristics and flow patterns changed. The wing with the thin, subsonic-type section showed leading-edge separation at angle of attack of about 6° ; whereas the wing with the modified double-wedge section showed such separation at about 4° . It was also noted from the pressure distributions of the wing with the subsonic section that the leading-edge separation was followed by a vortex type of flow of the same nature but of less intensity than that which occurred on the wing with the modified double-wedge section. A similar comparison cannot be made with a wing having a true double-wedge section due to the unavailability of pressure-distribution data for such a wing. However, it is known from force-test results (NACA RM A7H28, 1947) that the effect of the modifications of the double-wedge section was only minor.

INTRODUCTION

A detailed study of the load distribution at low Mach numbers and high Reynolds numbers on a triangular wing having modified double-wedge

[REDACTED] UNCLASSIFIED

sections has been reported in reference 1. Therein, data were also given to show the load distribution of a wing of similar plan form but having thin, subsonic-type airfoil sections. These latter data, however, were very limited in scope and, since it has recently been indicated that at moderate supersonic speeds the subsonic airfoil section is desirable, it was considered useful to make available a more complete set of data for the case of a triangular wing having a thin, subsonic-type airfoil section.

In order to afford a comparison of the effects of airfoil section alone, a triangular wing was chosen having the same plan form and thickness as that wing the characteristics of which were reported in reference 1. Since the investigation was directed primarily at defining the load distribution of such a wing, detailed pressure distributions were obtained throughout the angle-of-attack range for three deflections of a trailing-edge flap. It is the purpose of this report to present these loading data but without detailed analysis. Together with references 1 and 2 this report makes available loading data on low-aspect-ratio triangular wings with either thin supersonic, thick subsonic, or thin subsonic-type airfoil sections.

SYMBOLS AND COEFFICIENTS

The symbols and coefficients used in this report are defined as follows:

- A aspect ratio $\left(\frac{b^2}{S}\right)$
- α free-stream angle of attack with reference to the wing-chord plane, degrees
- b wing span, feet
- b_f flap semispan, feet
- c wing chord, measured parallel to wing center line, feet
- c_{av} average wing chord $\left(\frac{S}{b}\right)$, feet
- \bar{c} mean aerodynamic chord, measured parallel to wing center line

$$\left(\frac{\int_0^{b/2} c^2 dy}{\int_0^{b/2} c dy}\right), \text{ feet}$$

\bar{c}_f root-mean-square chord of the flap aft of the hinge line

$$\left(\sqrt{\frac{\int_0^{b_f} c_f^2 dy}{b_f}} \right), \text{ feet}$$

c_l section lift coefficient $\left(\frac{\text{section lift}}{qc} \right)$

C_D wing drag coefficient $\left(\frac{\text{wing drag}}{qS} \right)$

C_L wing lift coefficient $\left(\frac{\text{wing lift}}{qS} \right)$

C_m wing pitching-moment coefficient about $0.25 \bar{c}$

$$\left(\frac{\text{wing pitching moment}}{qS\bar{c}} \right)$$

C_h flap hinge-moment coefficient $\left(\frac{\text{hinge moment}}{q b_f c_f^2} \right)$

$\frac{c_l c}{C_L c_{av}}$ span loading coefficient

δ_f flap deflection, measured perpendicular to hinge line, degrees
(subscript n denotes nominal deflection)

p free-stream static pressure, pounds per square foot

p_l local static pressure, pounds per square foot

P pressure coefficient $\left(\frac{p_l - p}{q} \right)$

q free-stream dynamic pressure, pounds per square foot

S wing area, square feet

S_f flap area, square feet

x distance along chord from leading edge, feet
 y distance along wing semispan from wing center line, feet

APPARATUS

The wing used in these tests was of triangular plan form with an aspect ratio of 2 which gave a leading-edge sweepback of 63.43° . The airfoil sections, taken parallel to the plane of symmetry, were NACA 0005 modified to the extent that aft of the 67-percent-chord point the sections were faired to the trailing edge by straight lines. Coordinates of the modified section are given in table I. The wing was equipped with full-span, constant-chord, plain trailing-edge flaps. The flap gaps were sealed for all the tests with cellulose tape at the upper and lower surfaces of the wing to form a smooth contour. Relevant wing dimensions are given in table II and in figure 1; figure 2 shows the model as mounted in the Ames 40- by 80-foot wind tunnel.

Wing pressures were measured through pressure orifices located on both upper and lower surfaces along six stations parallel to the plane of symmetry. (See fig. 1.)

TESTS

Pressure distribution, force data, and flap hinge moment were obtained at zero sideslip through an angle-of-attack range from -2° to $+37^\circ$. For all tests the dynamic pressure was 25 pounds per square foot resulting in a Reynolds number, based on the mean aerodynamic chord, of 15.3×10^6 . The Mach number was 0.13.

Data were obtained for three nominal flap deflections, 0° and $\pm 10^\circ$. Due to the flap load and the initial flap setting, the true deflection varied slightly from these nominal values. This variation, determined by means of static load-deflection measurements and flap hinge moments due to air load, is shown in figure 3. No attempt has been made to adjust the force or pressure data to constant flap angle since the primary interest was in the load distribution and not the integrated effect.

Reduction and Accuracy of Data

The measured static pressures on the wing were reduced to pressure coefficient form and plotted both perpendicular and parallel to their respective chords. The pressure coefficients are believed accurate

within ± 0.02 . Values of section lift coefficient, center of pressure, span-loading coefficient, and wing lift, drag, and pitching-moment coefficients were derived by means of mechanical integration and calculation and include the forces both parallel and perpendicular to the chord.

All the force data presented have been corrected for air-stream inclination and for wind-tunnel-wall effect, the latter correction being that for a wing of the same span but of rectangular plan form. In addition, the force-test drag and pitching-moment data have been corrected for support-strut interference. Angles of attack for the pressure data have been adjusted the same as was done for the force data. No other corrections were applied to the pressure data.

RESULTS AND DISCUSSION

The gross force characteristics of the wing are given in figure 4. These include lift, drag, pitching-moment, and flap hinge-moment coefficients for nominal flap deflections of 0° and $\pm 10^\circ$. Chordwise pressure distributions for each section and flap deflection are presented in figures 5, 6, and 7 for selected angles of attack to illustrate all significant changes in loading. These pressure distributions, together with similar ones at other angles of attack, have been integrated to obtain additional characteristics. Figure 8 compares the over-all wing characteristics as found from force-test measurements and from integration of the pressure data for zero flap deflection. It can be concluded from this that the pressure data are sufficiently complete to give an accurate picture of wing loadings. Figures 9 and 10, respectively, show the variation in section lift coefficient and section center-of-pressure location with angle of attack of the wing for each section and flap angle. The spanwise load distribution on the wing is shown for selected angles of attack and the three flap angles in figure 11.

In the main, these results show, when compared with the data of references 1, 3, and 4, that the change in airfoil section results in only minor changes in wing characteristics. The early appearance of leading-edge separation with subsequent formation of a vortex lying along the wing leading edge is evident as is the effect of this flow on the wing loading. Thus, most of the analysis given in reference 1 regarding the nature of the flow is directly applicable here with the only significant difference being the angle of attack or lift coefficient at which the flow pattern changes. However, the vortex type of flow which followed the occurrence of leading-edge separation does not appear to have been as strong as that which occurred on the wing with the modified double-wedge section. This is indicated by the lesser distortion of the chordwise pressure distributions for the present case. Under such circumstances, a detailed discussion of the loading or its changes with angle of attack is not believed warranted.

In considering the improvements resulting from the changes from a modified¹ double-wedge section (reference 1) to a subsonic-type section, it can be seen that they are restricted to the low lift-coefficient range. Whereas the modified double-wedge section showed (from examination of the pressure distribution) leading-edge separation at an angle of attack of about 4° (reference 1) the subsonic-type section considered herein did not show such separation until an angle of attack of about 6° .

Examination of the data obtained with the trailing-edge flaps deflected shows certain points of interest. From figure 4 it will be noted that, compared to the wing with flaps undeflected, at a given lift coefficient the drag was increased by negative flap deflections and reduced by positive flap deflections. The source of this drag change can be found from both the section lift-curve slope and the section pressure distributions. From these data, it can be seen that as the flap is increasingly deflected in a positive direction the section maximum lift for both unseparated (as indicated by a sudden discontinuity in the section lift-curve slope) and separated (highest section lift coefficient reached) flow conditions is increased, with the effect becoming much stronger toward the tip. For the section at 90-percent semispan, only a shift in the angle of zero lift without any change in maximum lift would have been expected since at this section it is the whole wing chord that is being deflected. An explanation of the changes in maximum lift of this section is not presently available.

Ames Aeronautical Laboratory,
National Advisory Committee for Aeronautics,
Moffett Field, Calif.

¹Symmetrical double-wedge section modified by rounding its leading-edge and maximum-thickness ridges.

REFERENCES

1. Anderson, Adrien E.: Chordwise and Spanwise Loadings Measured at Low Speed on Large Triangular Wings. NACA RM A9B17, 1949. 1115.5
-126
2. Wick, Bradford H.: Chordwise and Spanwise Loadings Measured at Low Speed on a Triangular Wing Having an Aspect Ratio of Two and an NACA 0012 Airfoil Section. NACA TN 1650, 1948. 11113
NACA 0012/1
3. Anderson, Adrien E.: An Investigation at Low Speed of a Large-Scale Triangular Wing of Aspect Ratio Two. - I. Characteristics of a Wing Having a Double-Wedge Airfoil Section With Maximum Thickness at 20-Percent Chord. NACA RM A7F06, 1947.
4. Anderson, Adrien E.: An Investigation at Low Speed of a Large-Scale Triangular Wing of Aspect Ratio Two. - II. The Effect of Airfoil Section Modifications and the Determination of the Wake Downwash. NACA RM A7H28, 1947.

TABLE I.— COORDINATES OF THE NACA 0005 (MODIFIED) SECTION

Station (percent chord)	Ordinate (percent chord)
0	0
1.25	.789
2.50	1.089
5.00	1.481
7.50	1.750
10.00	1.951
15.00	2.228
20.00	2.391
25.00	2.476
30.00	2.501
40.00	2.419
50.00	2.206
60.00	1.902
67.00	1.650
70.00	1.500
80.00	1.000
90.00	.500
100.00	0

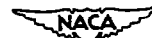
L.E. radius: 0.275 percent chord

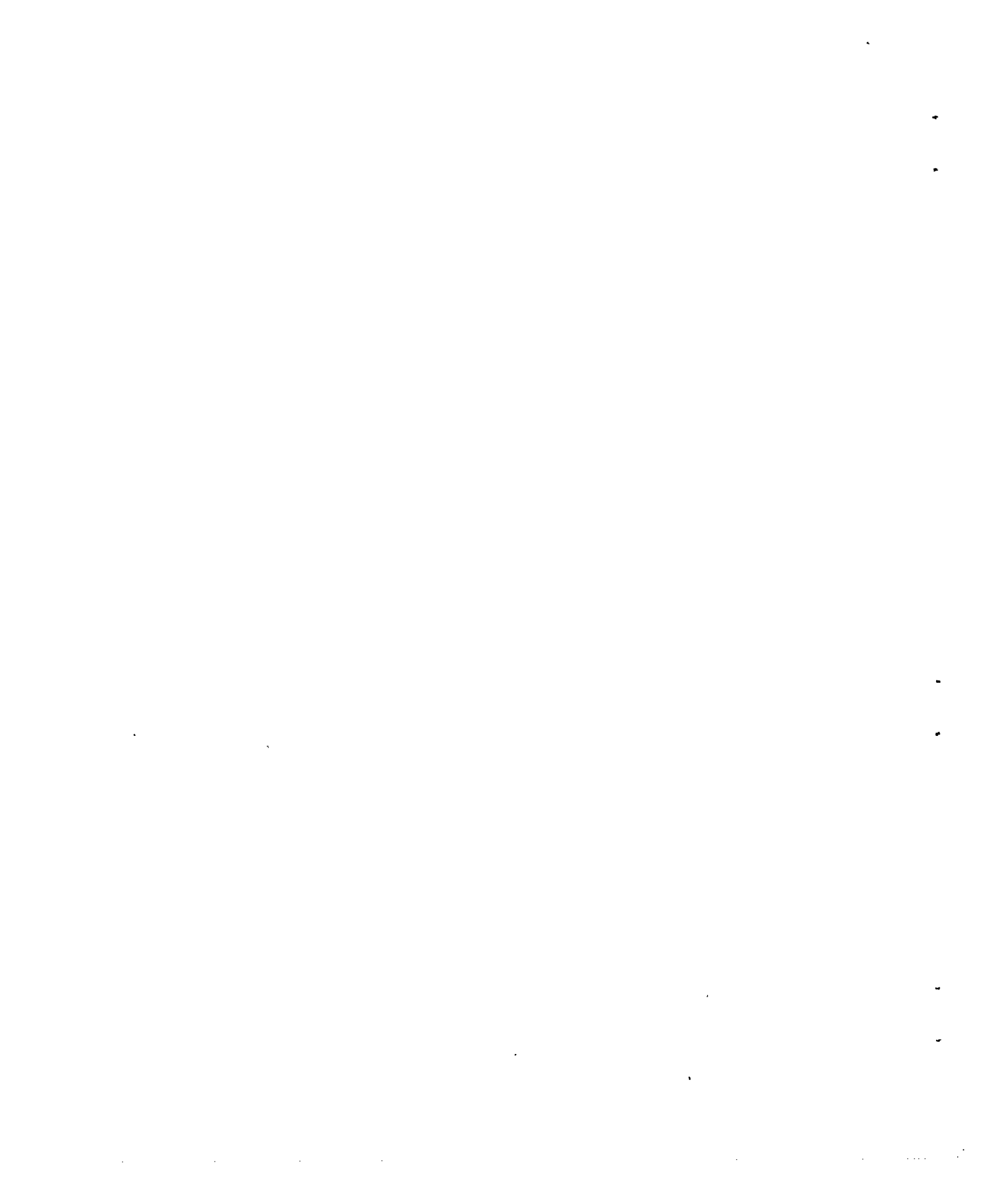


TABLE II.- GEOMETRIC DATA OF MODEL USED

Wing	
Area, square feet	312.5
Span, feet	25.00
Mean aerodynamic chord, feet	16.67
Aspect ratio	2
Taper ratio	0
Flap	
Area, square feet	62.5
Semispan, feet	12.23
Chord, feet	2.67
Root-mean-square chord, feet	2.55

$62.5 / 312.5 = 20\%$







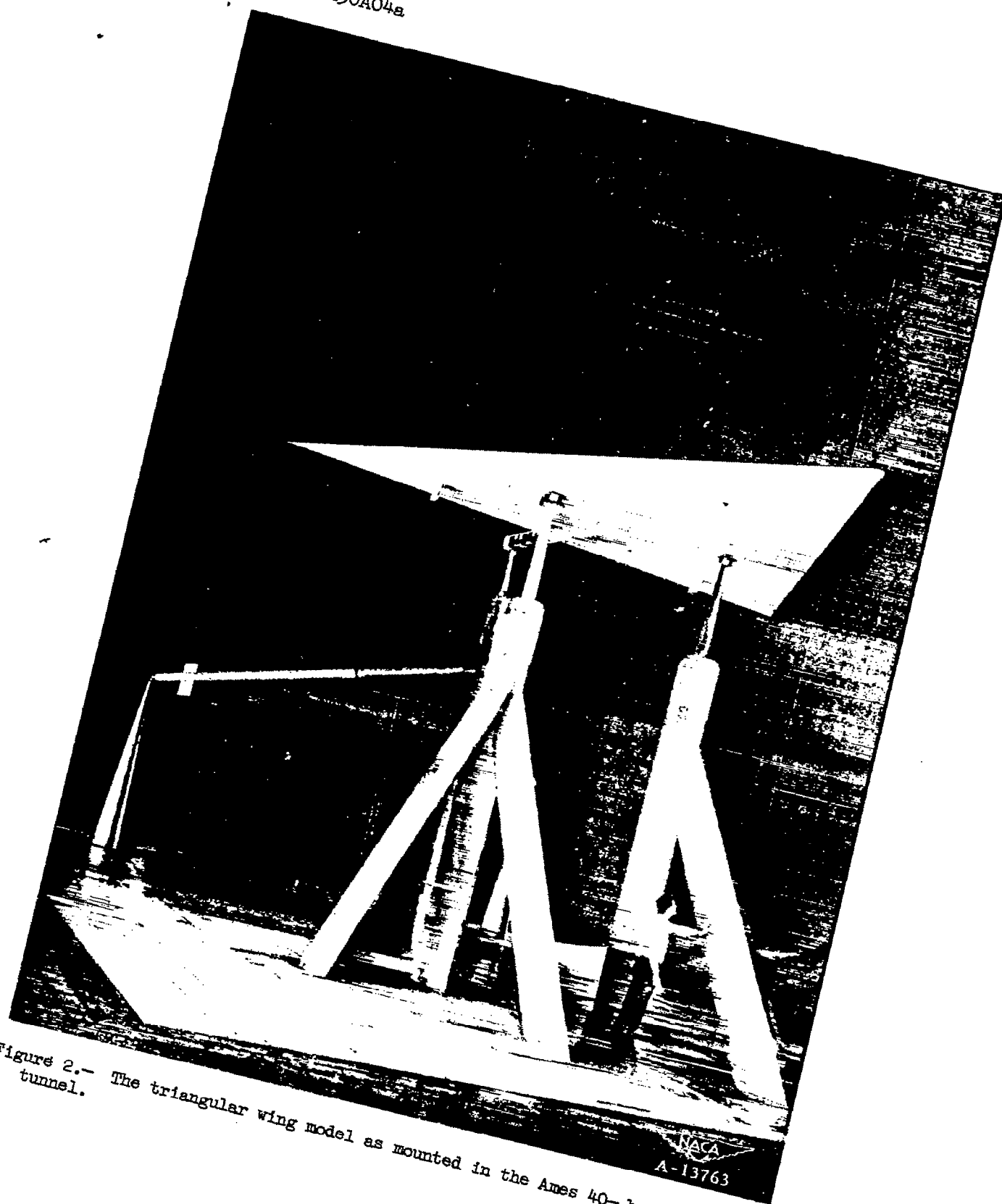
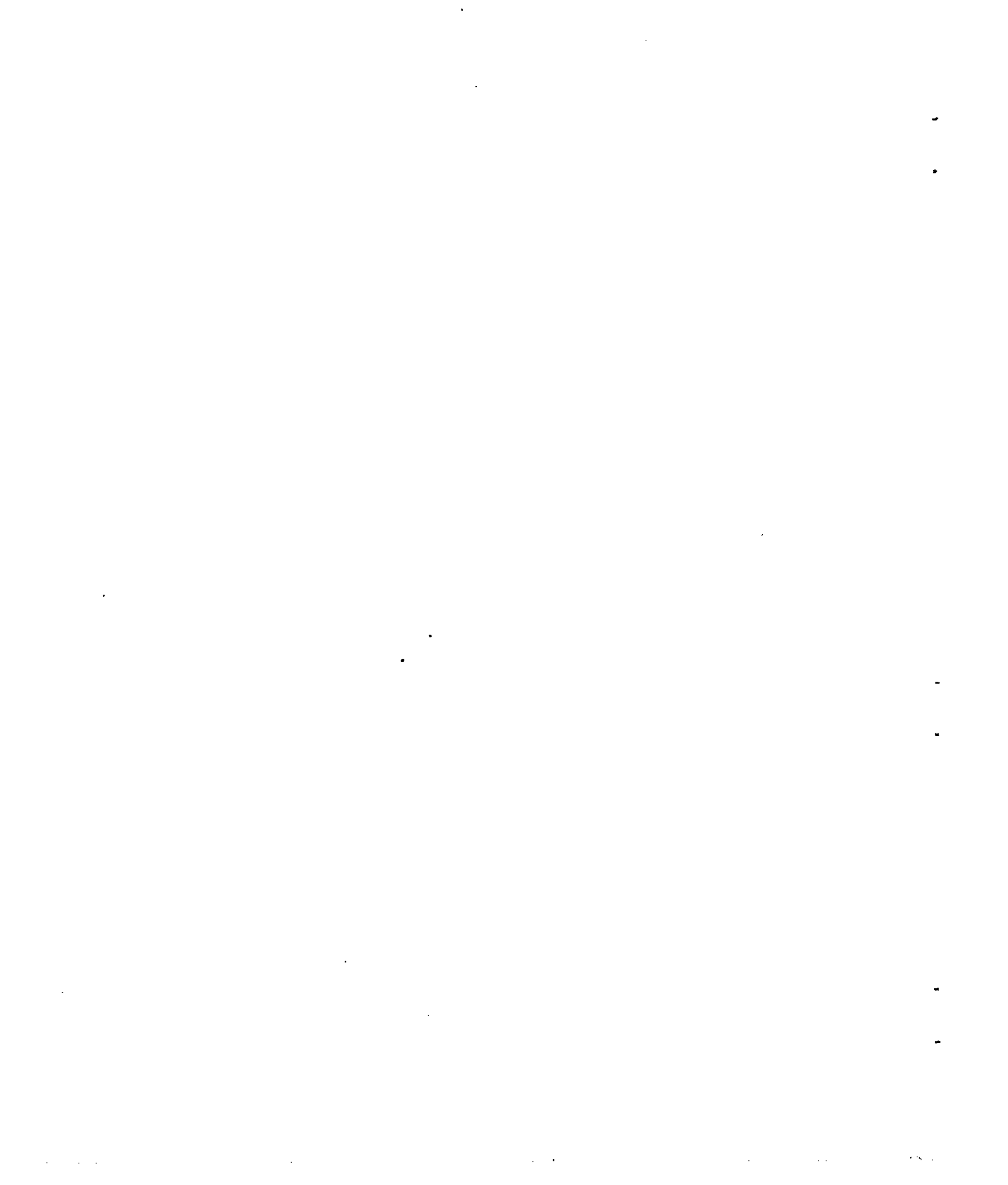


Figure 2.- The triangular wing model as mounted in the Ames 40- by 80-foot wind tunnel.



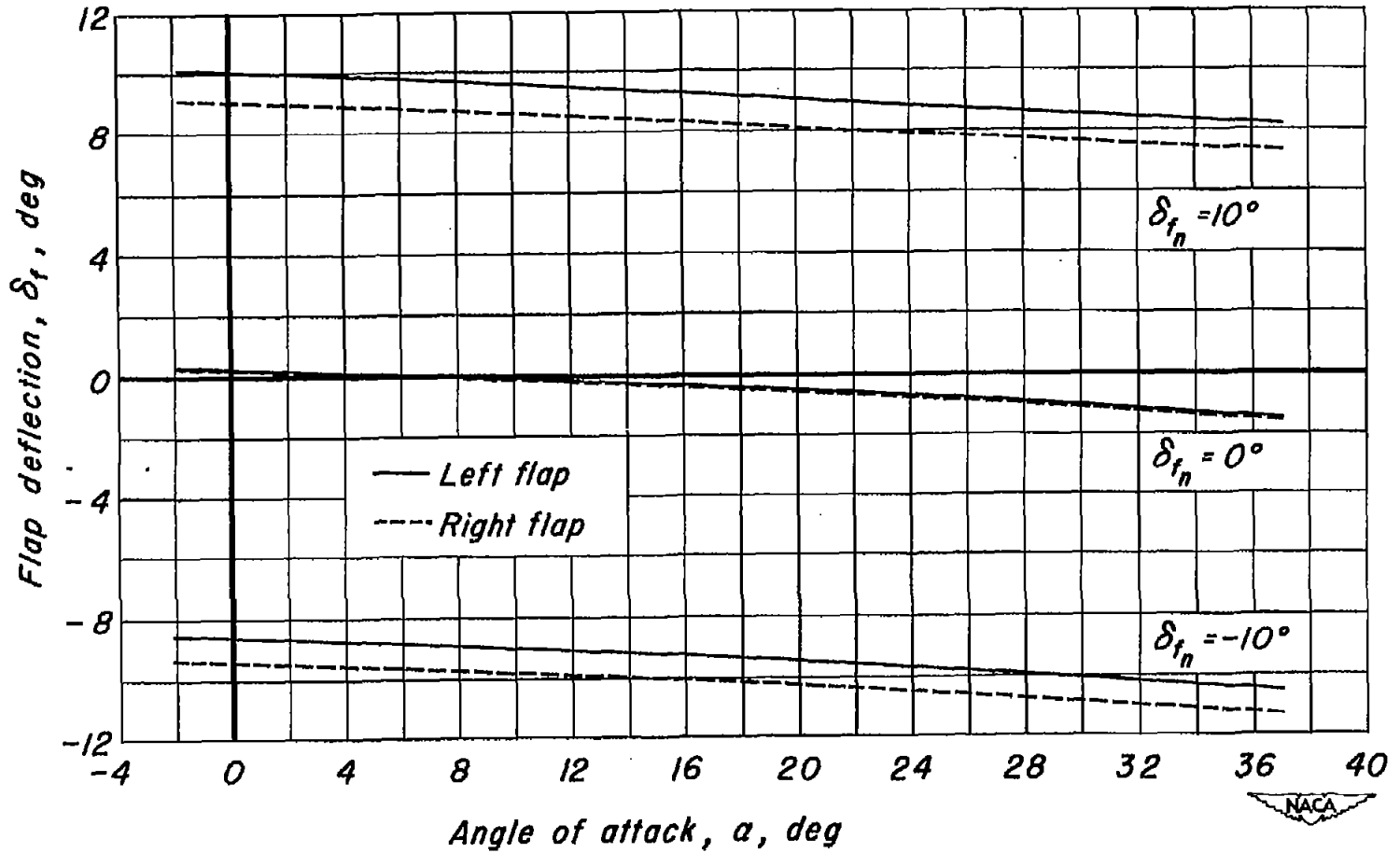
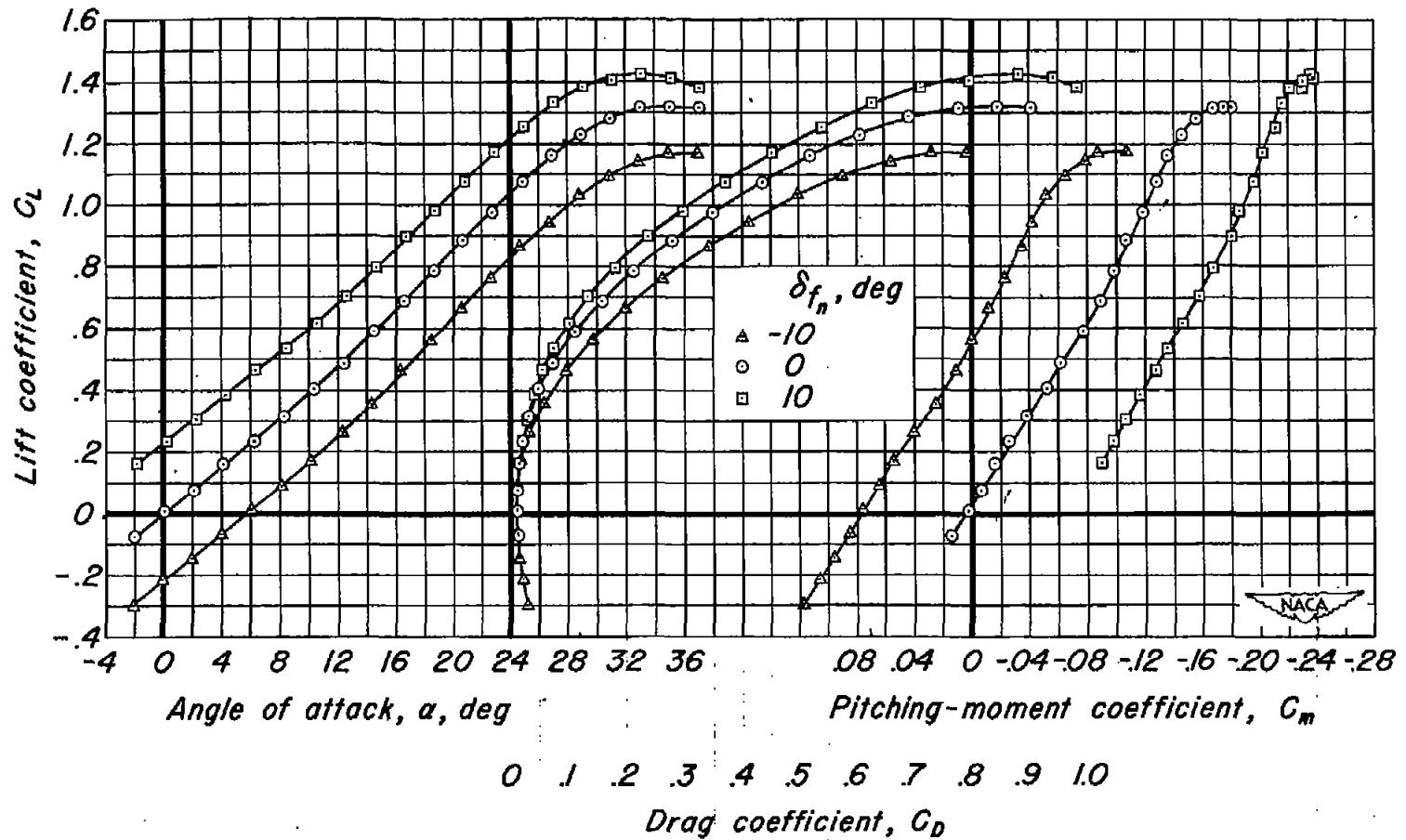
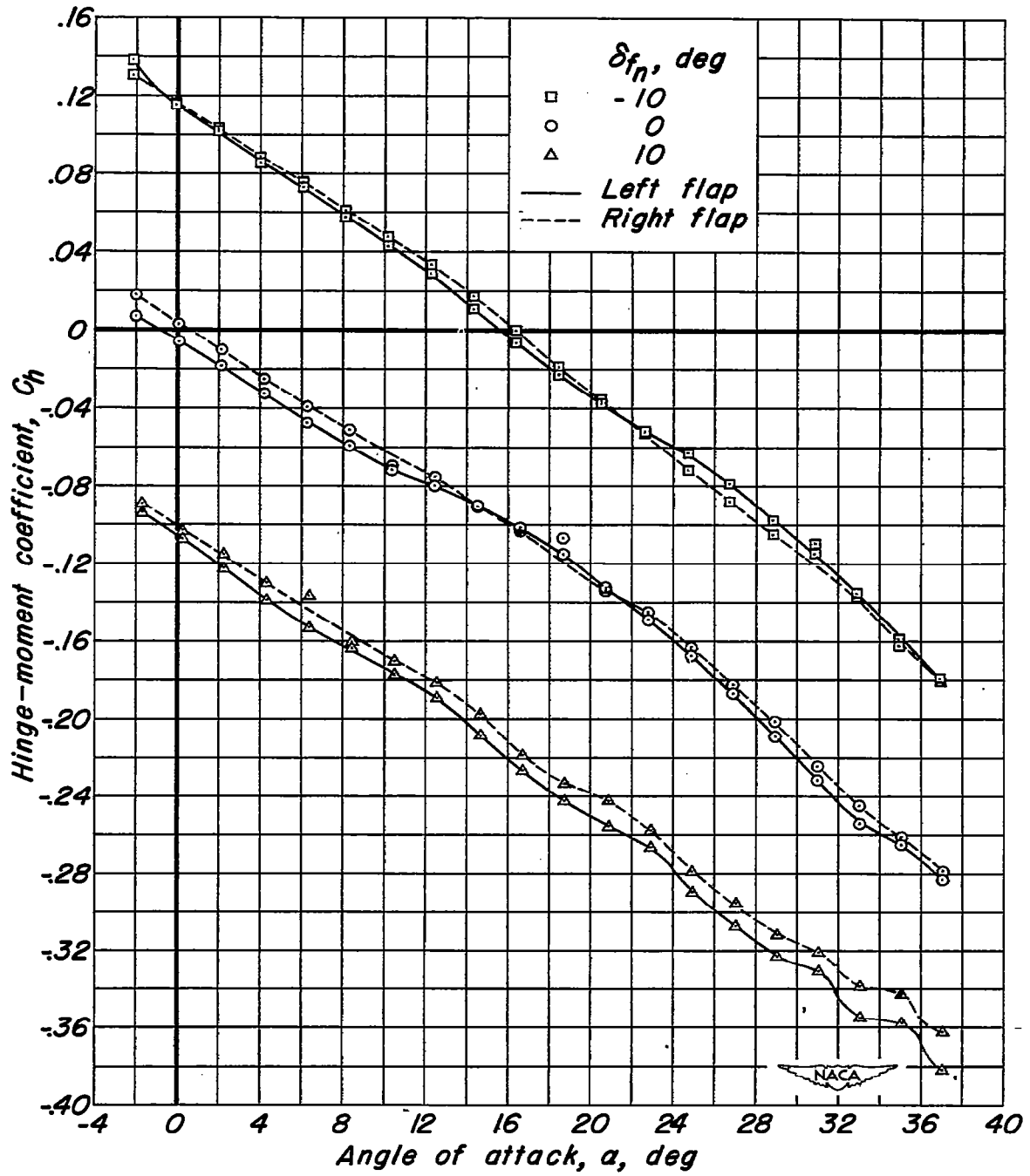


Figure 3.- Variation of the flap deflection with angle of attack. q , 25 lb/sq ft.



(a) C_L vs α , C_D , C_m .

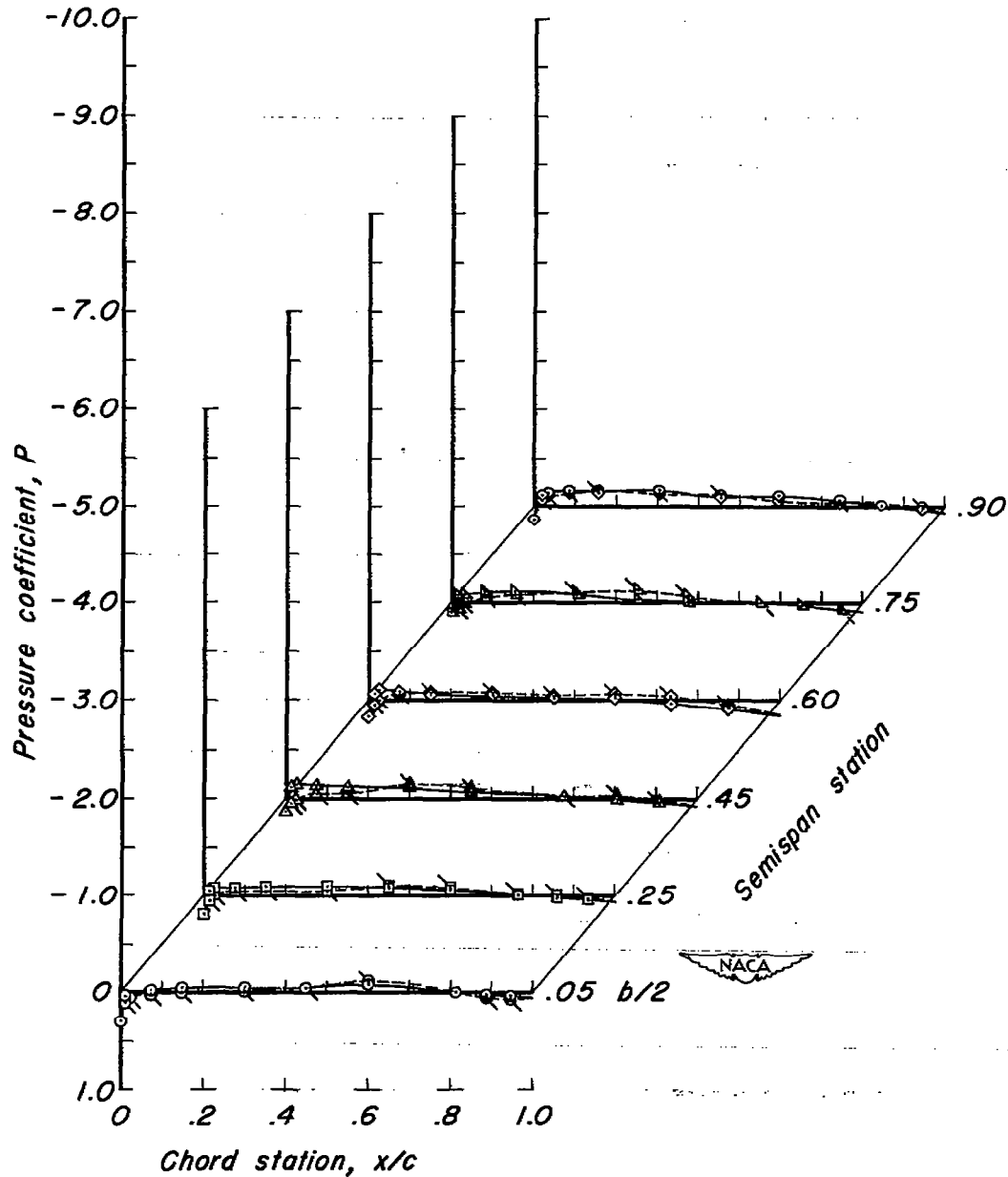
Figure 4.- Force test results.



(b) C_h vs a .

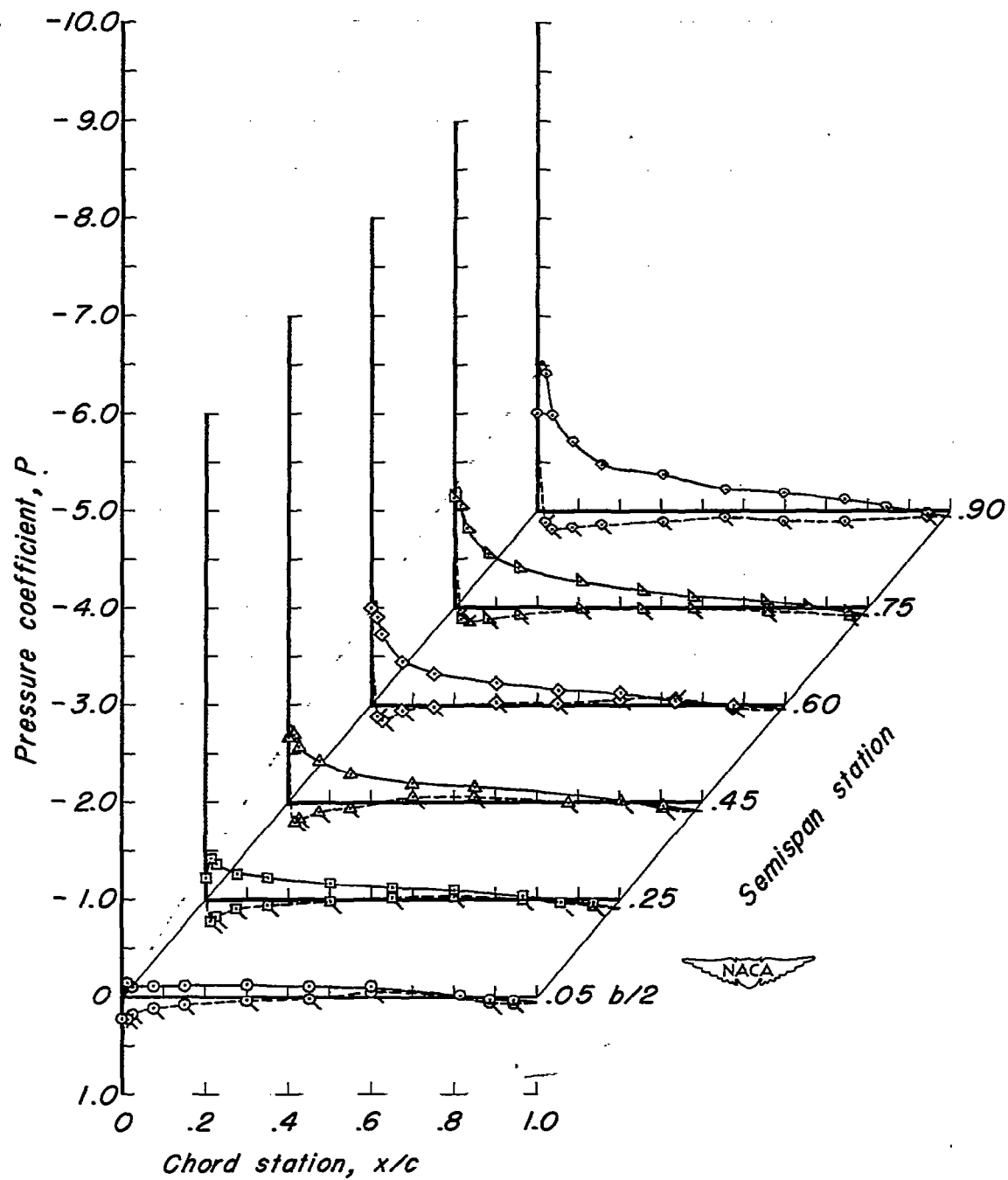
Figure 4.- Concluded.

Flagged symbols and dashed curves
indicate lower surface pressures.



(a) $\alpha, 0.1^\circ$.

Figure 5.- Pressure distribution along chord for various angles of attack. $\delta_{fn}, 0^\circ$.



(b) $\alpha, 4.2^\circ$.

Figure 5.- Continued.

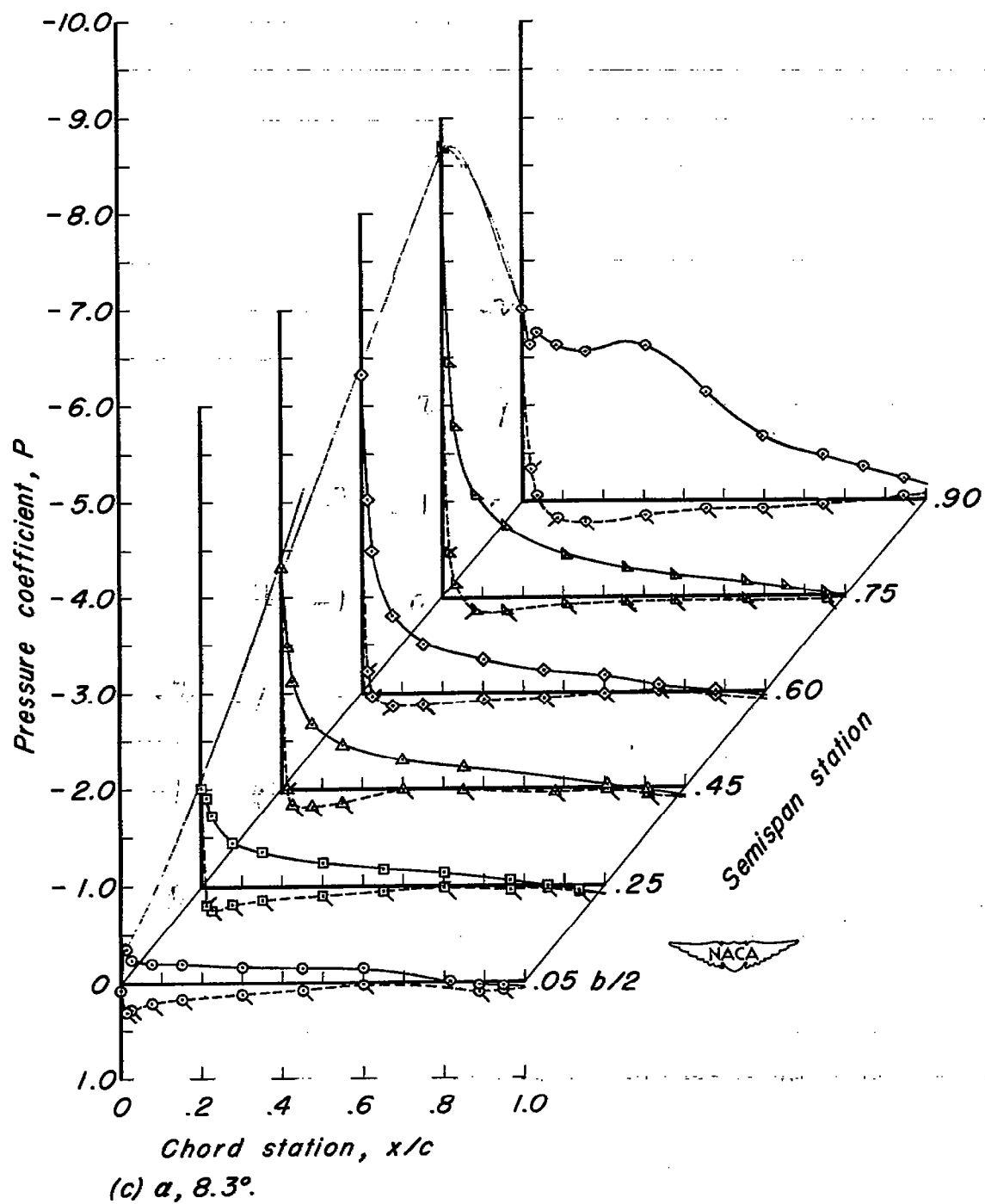
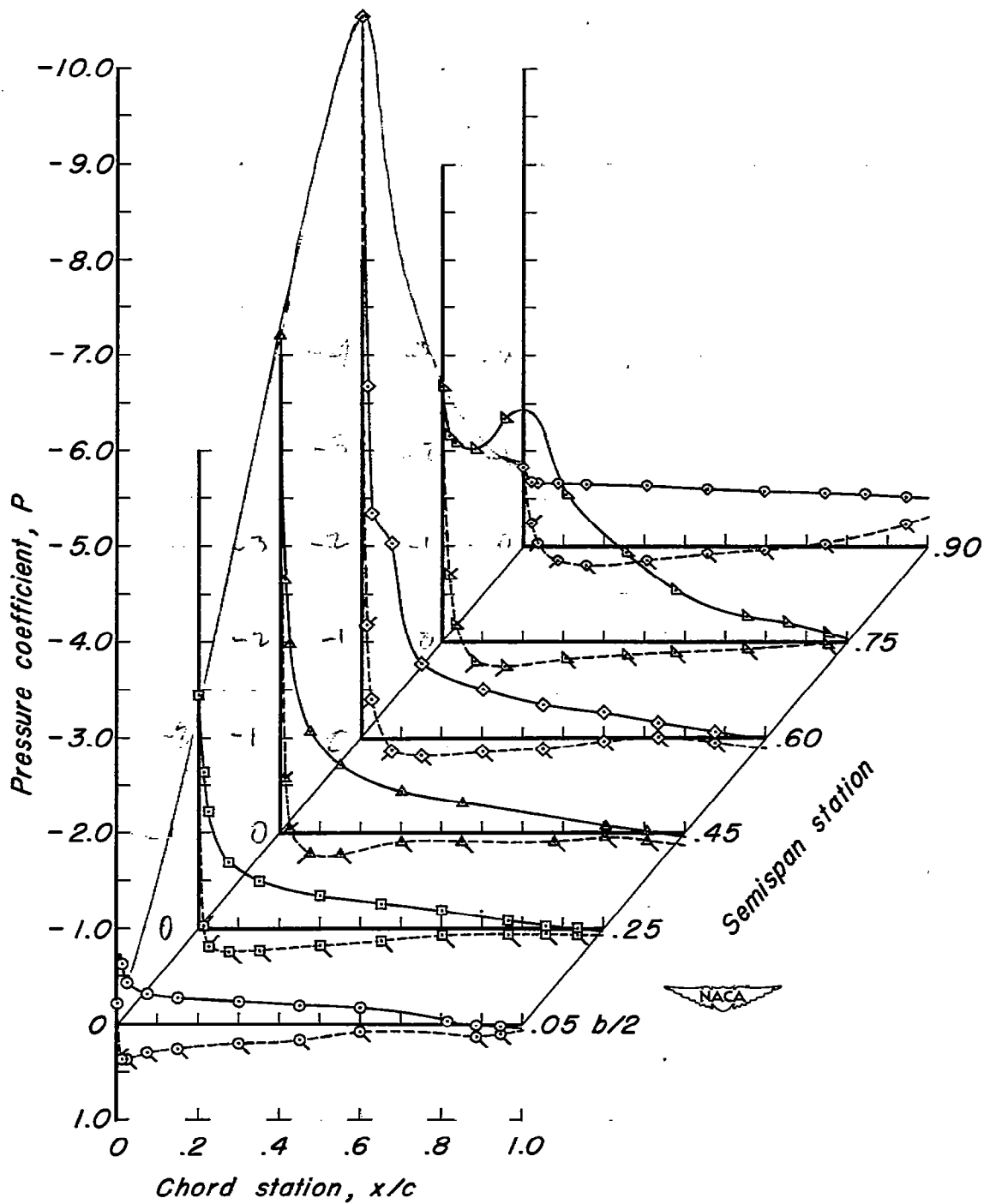


Figure 5.- Continued.



(d) $\alpha, 12.4^\circ$.

Figure 5. - Continued.

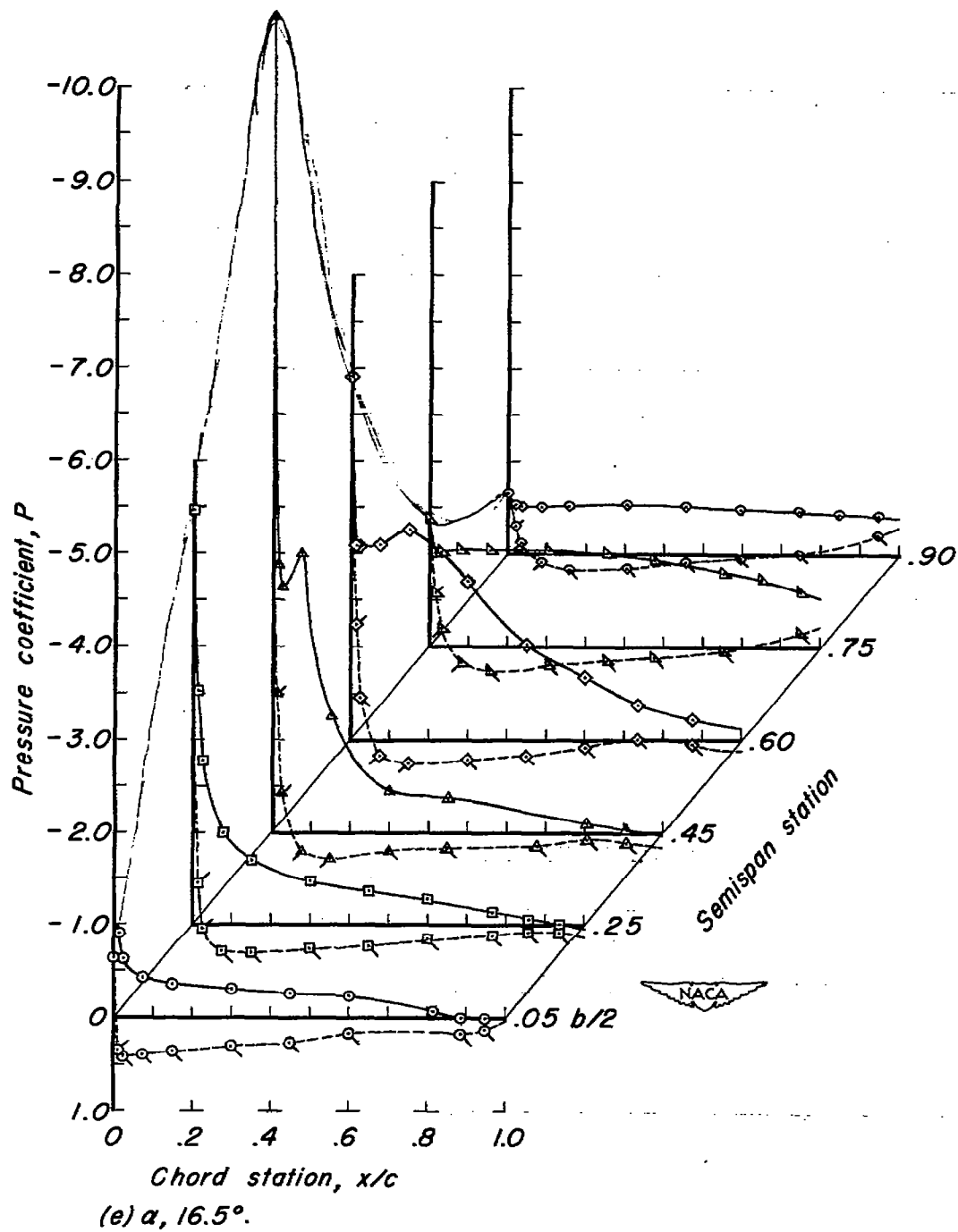


Figure 5.- Continued.

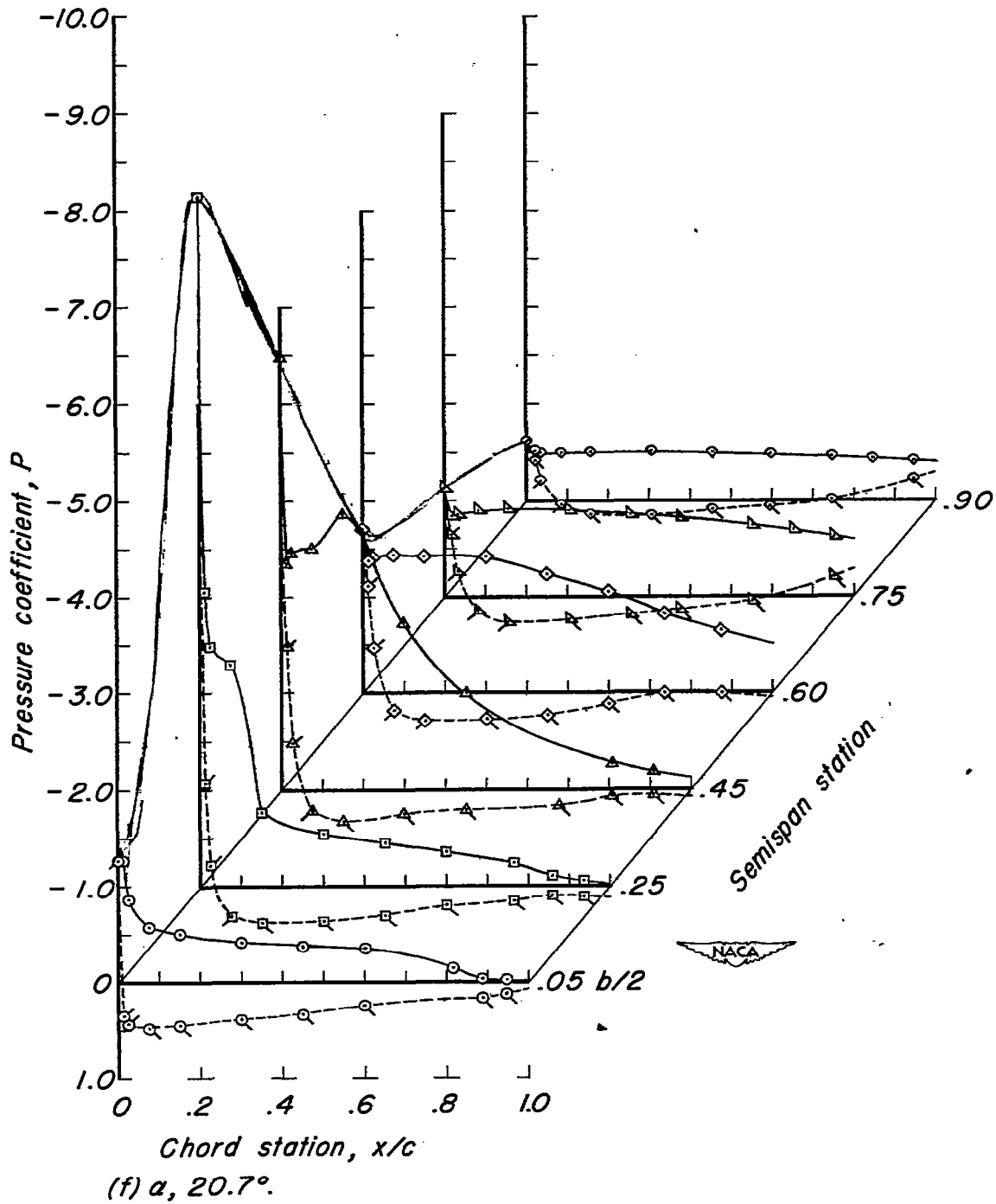


Figure 5.- Continued.

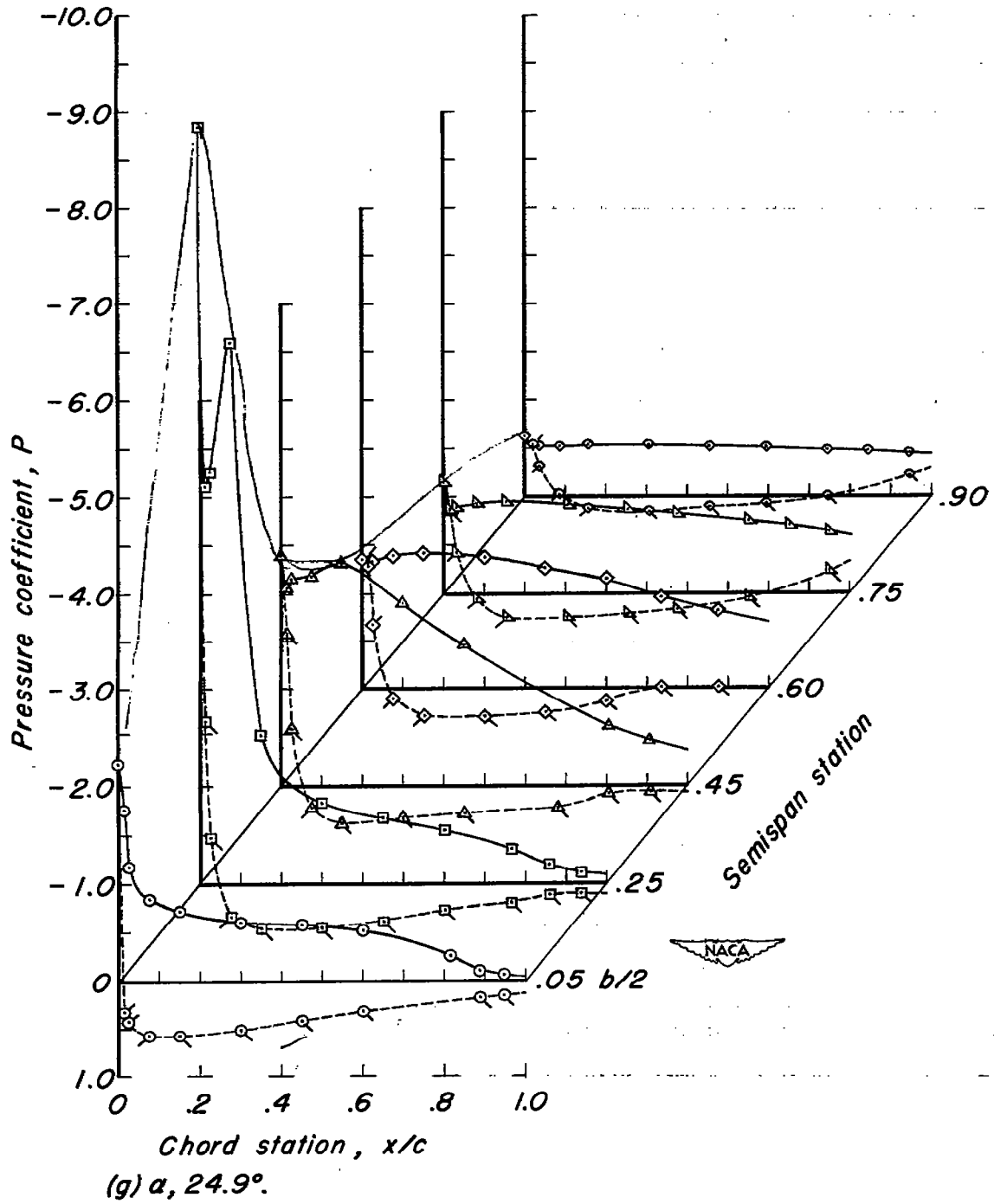


Figure 5.—Continued.

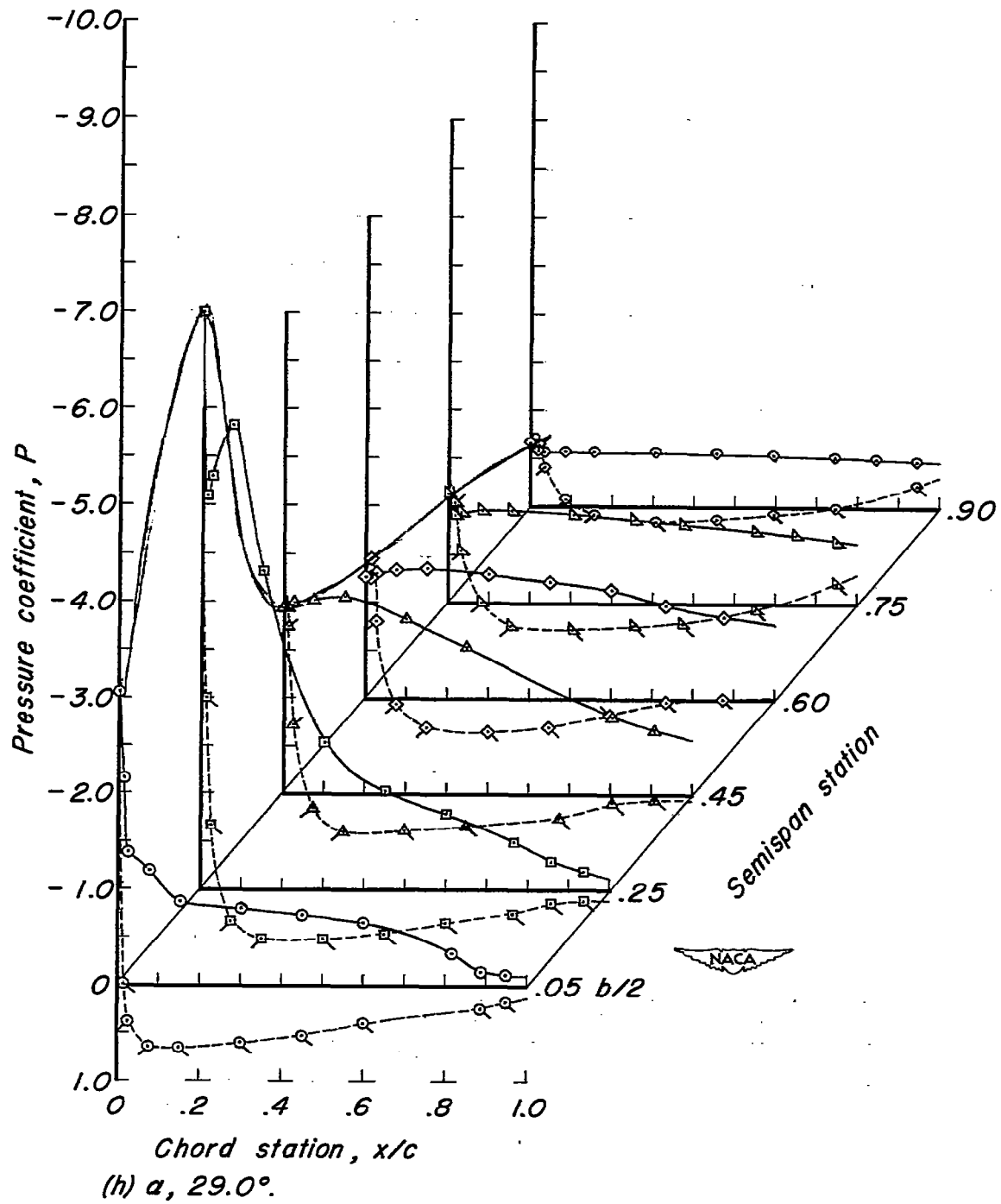
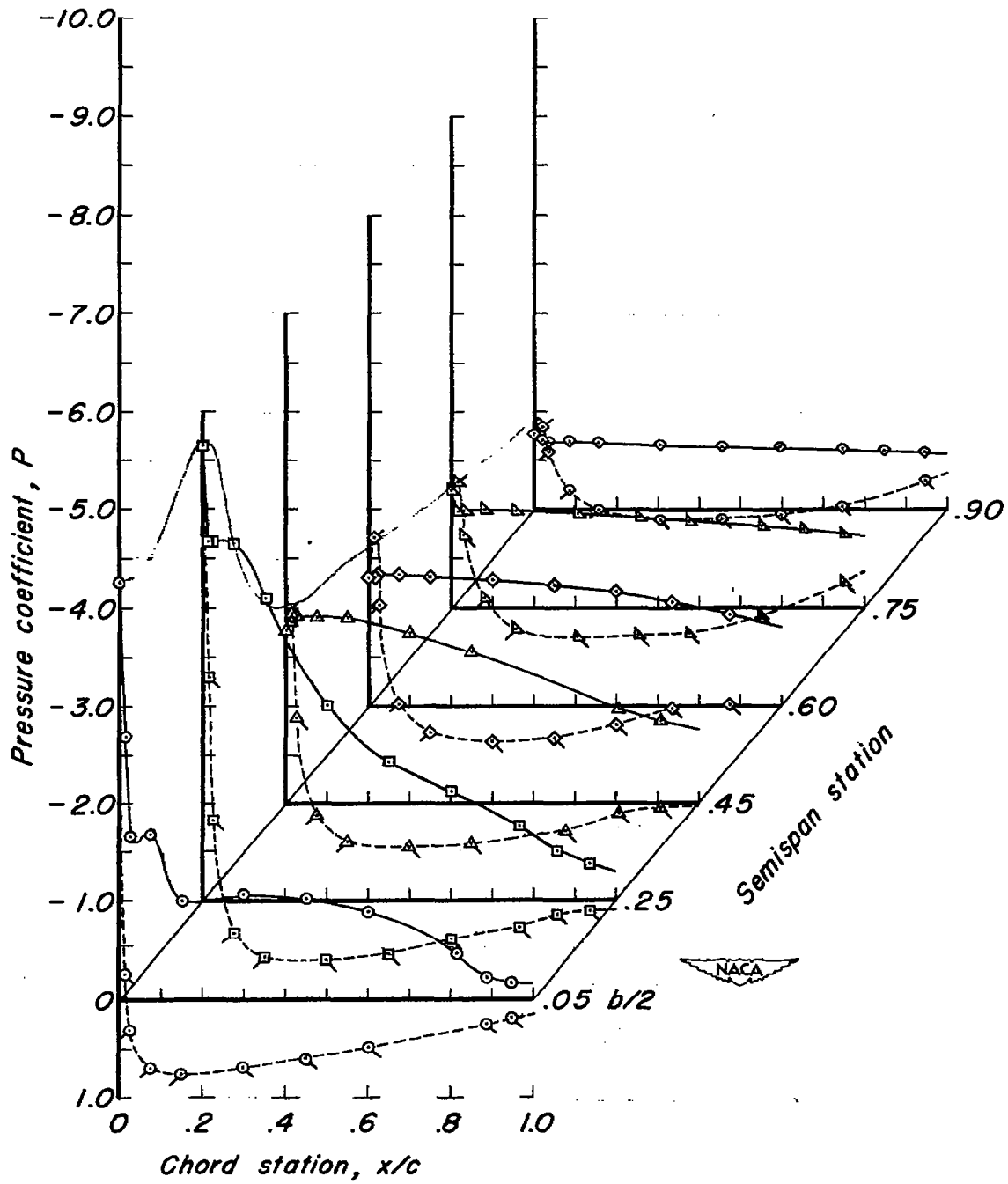
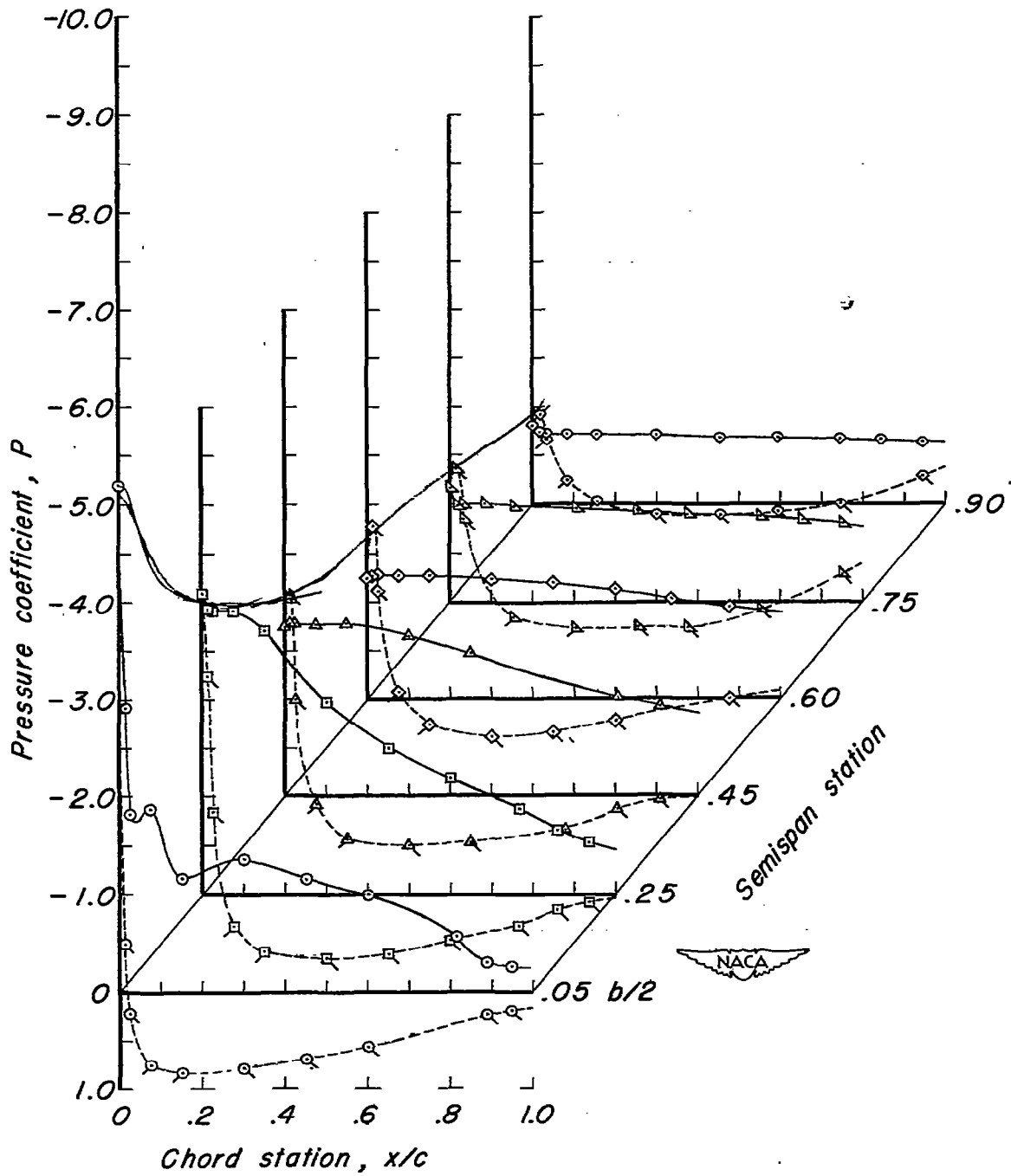


Figure 5.- Continued.



(i) α , 33.0° .

Figure 5.- Continued.



(j) $\alpha, 37.0^\circ$.

Figure 5.- Concluded.

Flagged symbols and dashed curves indicate lower surface pressures.

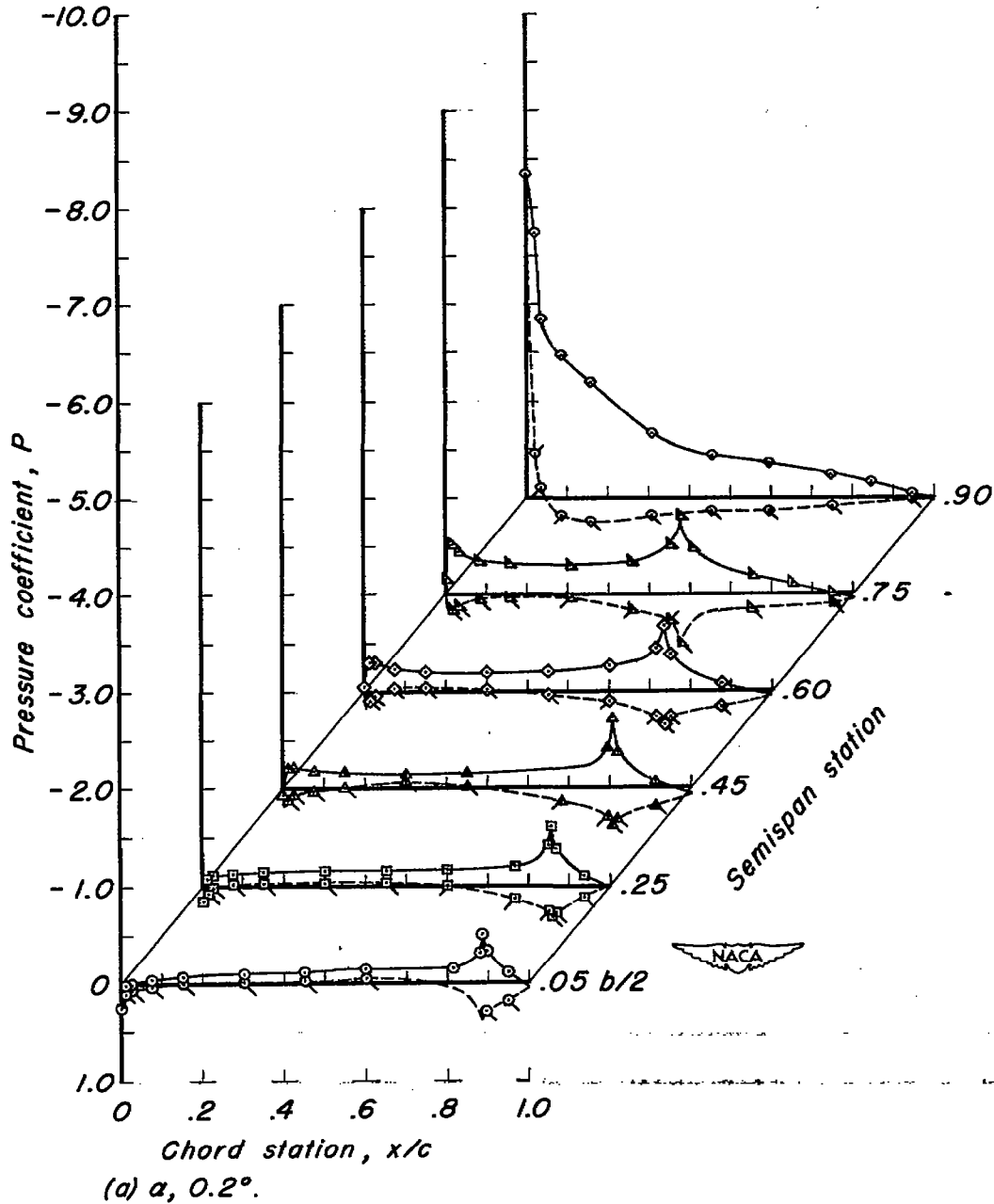
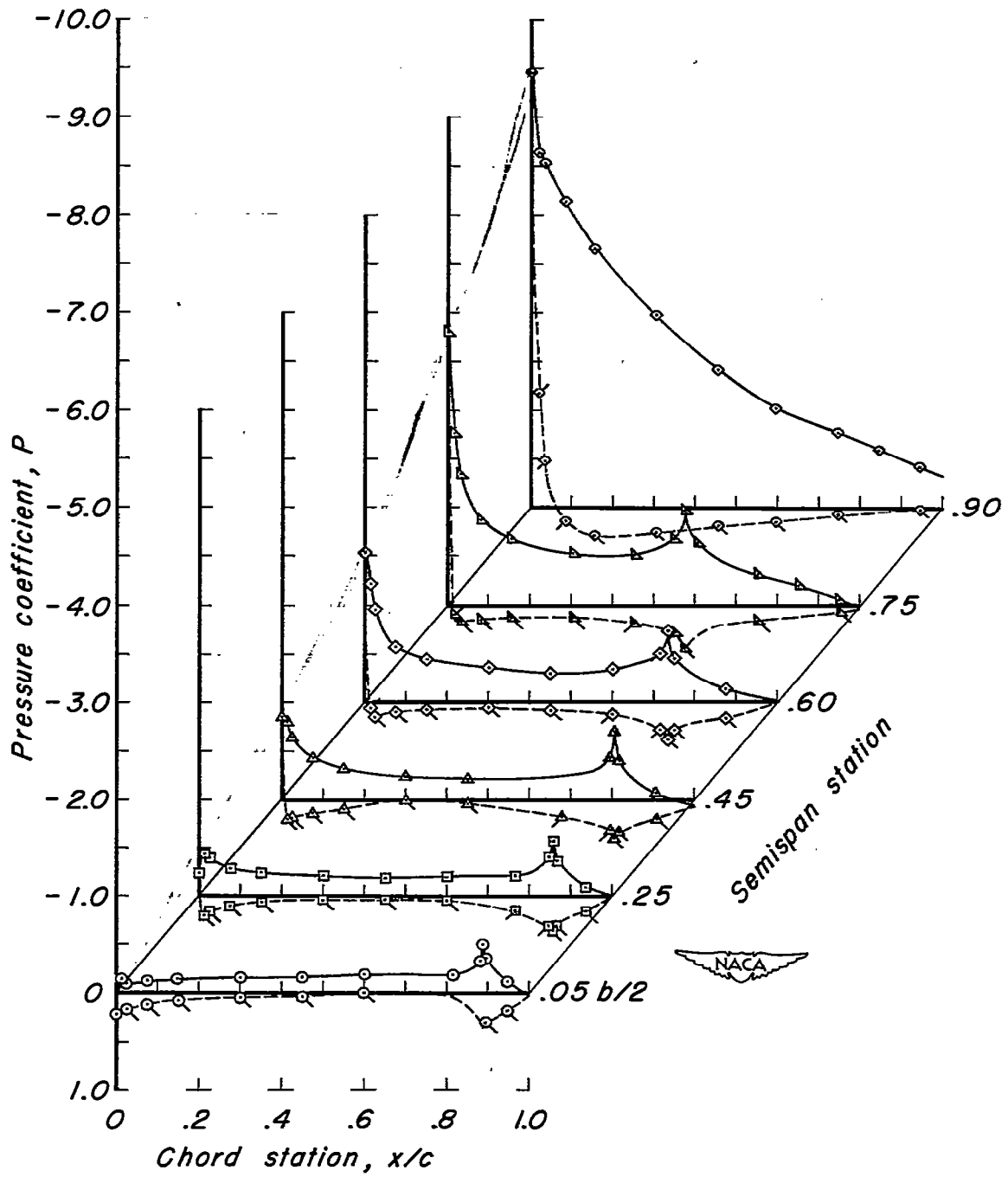
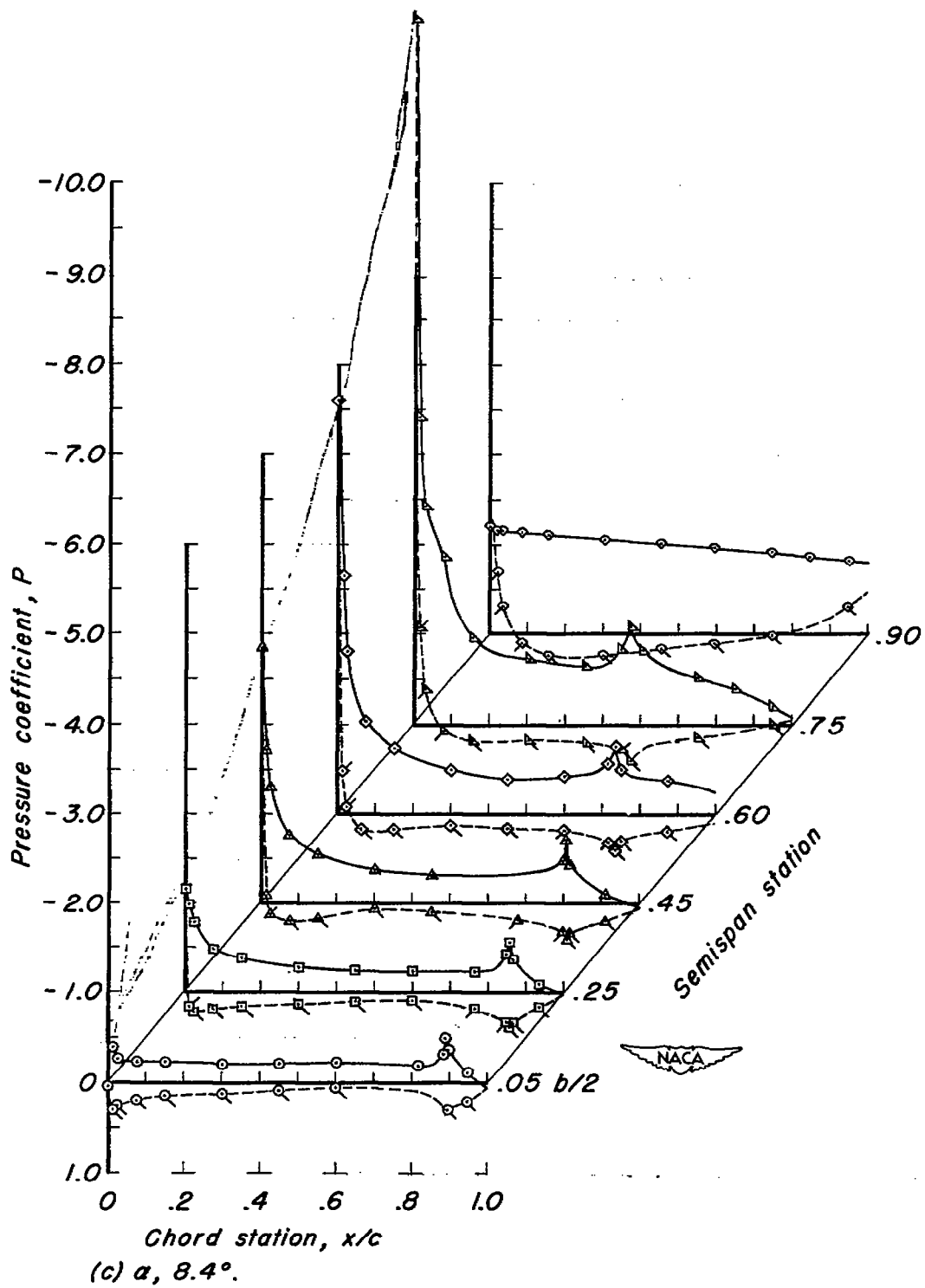


Figure 6.- Pressure distribution along chord for various angles of attack. $\delta_{f_n}, 10^\circ$.



(b) $\alpha, 4.3^\circ$.

Figure 6.- Continued.



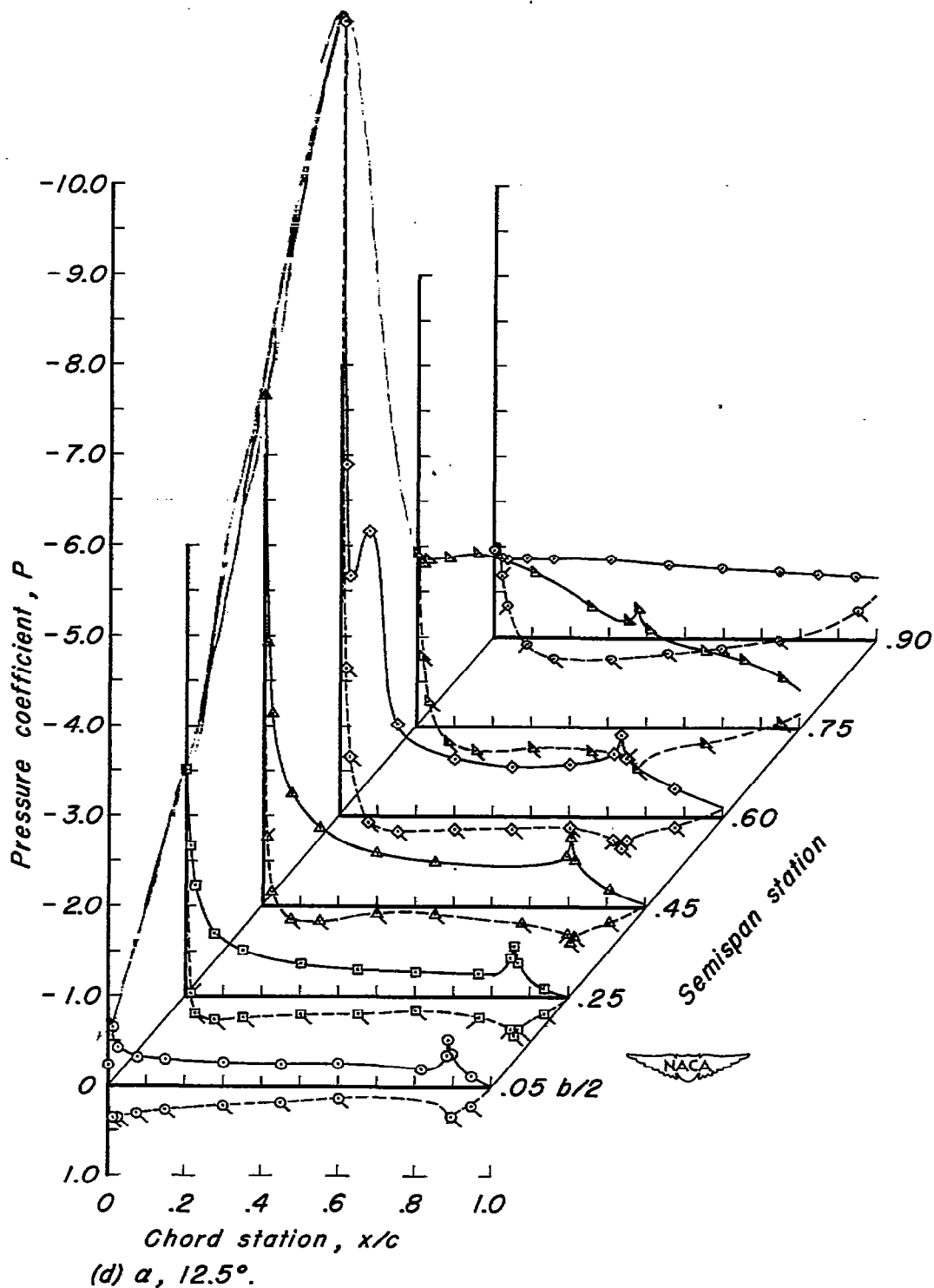


Figure 6.- Continued.

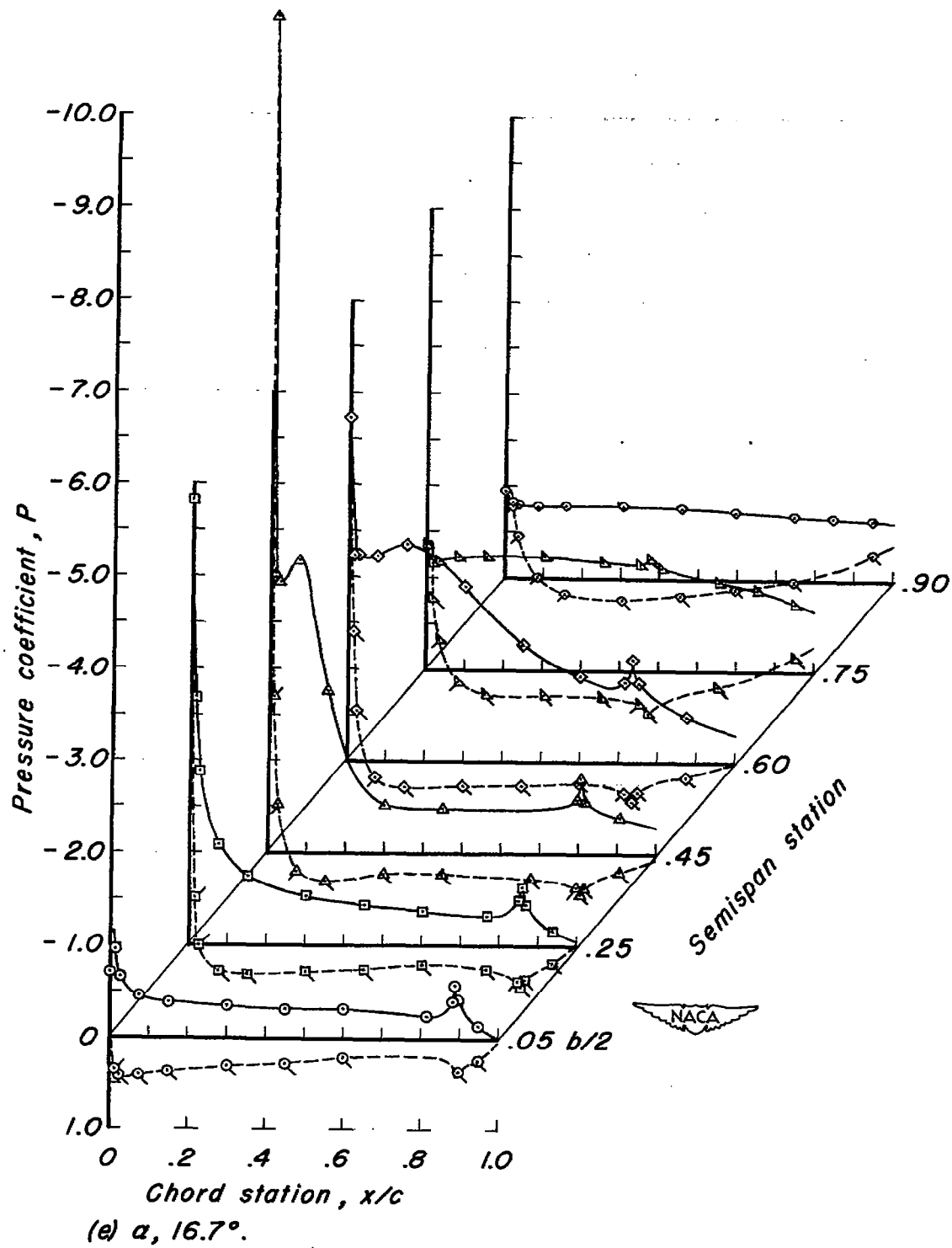
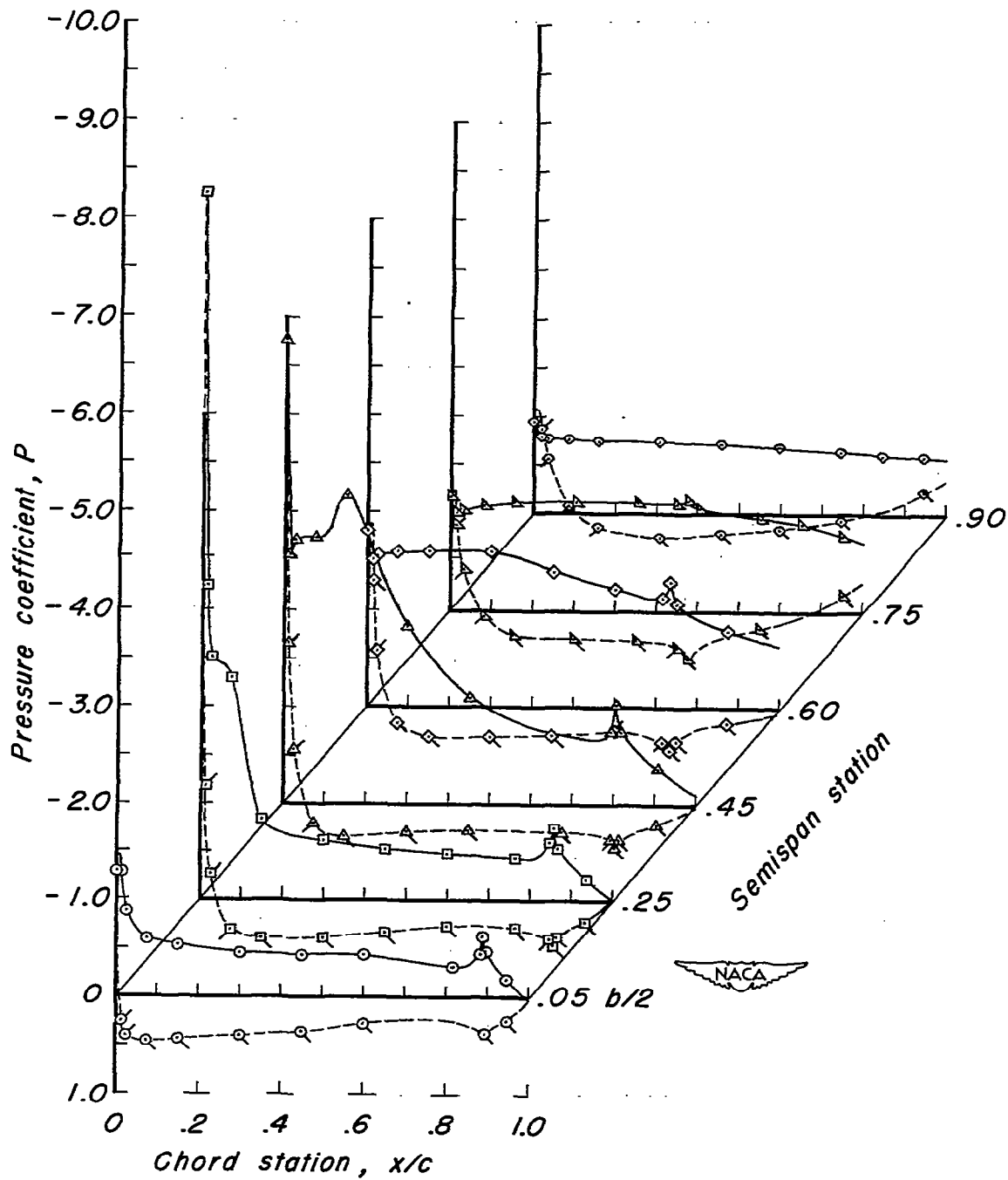


Figure 6.- Continued.



(f) α , 20.8° .

Figure 6.- Continued.

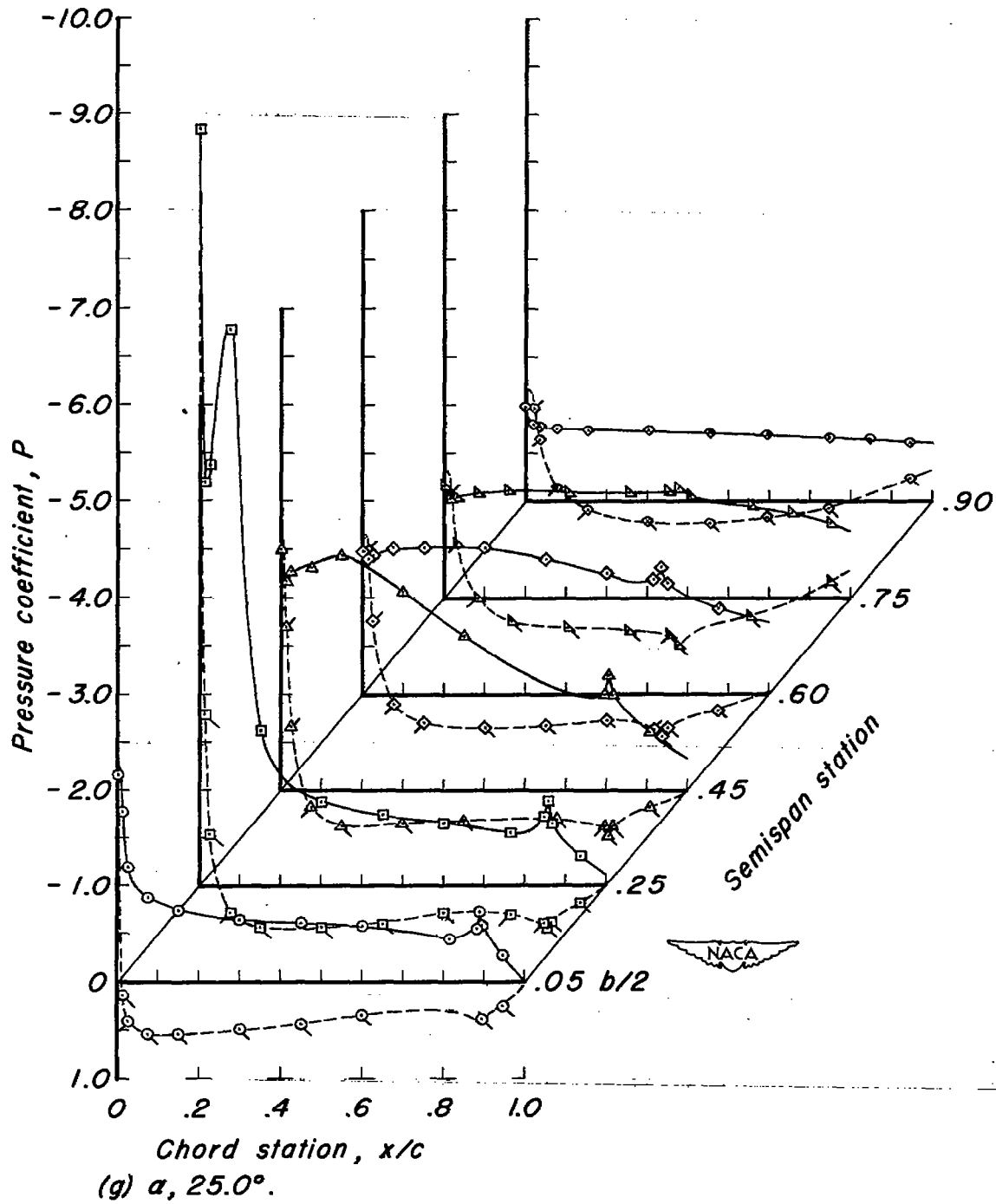


Figure 6.- Continued.

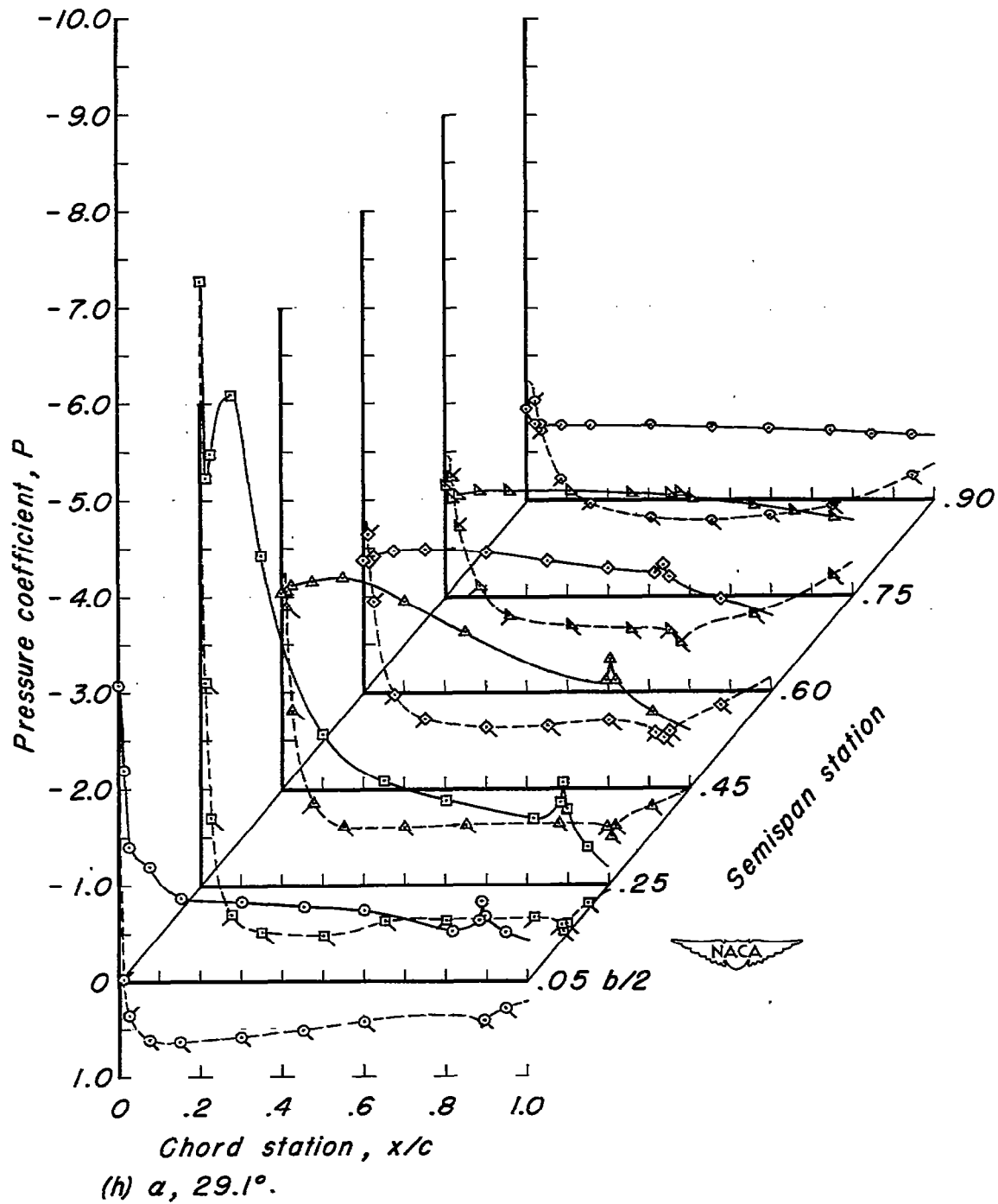


Figure 6.-Continued.

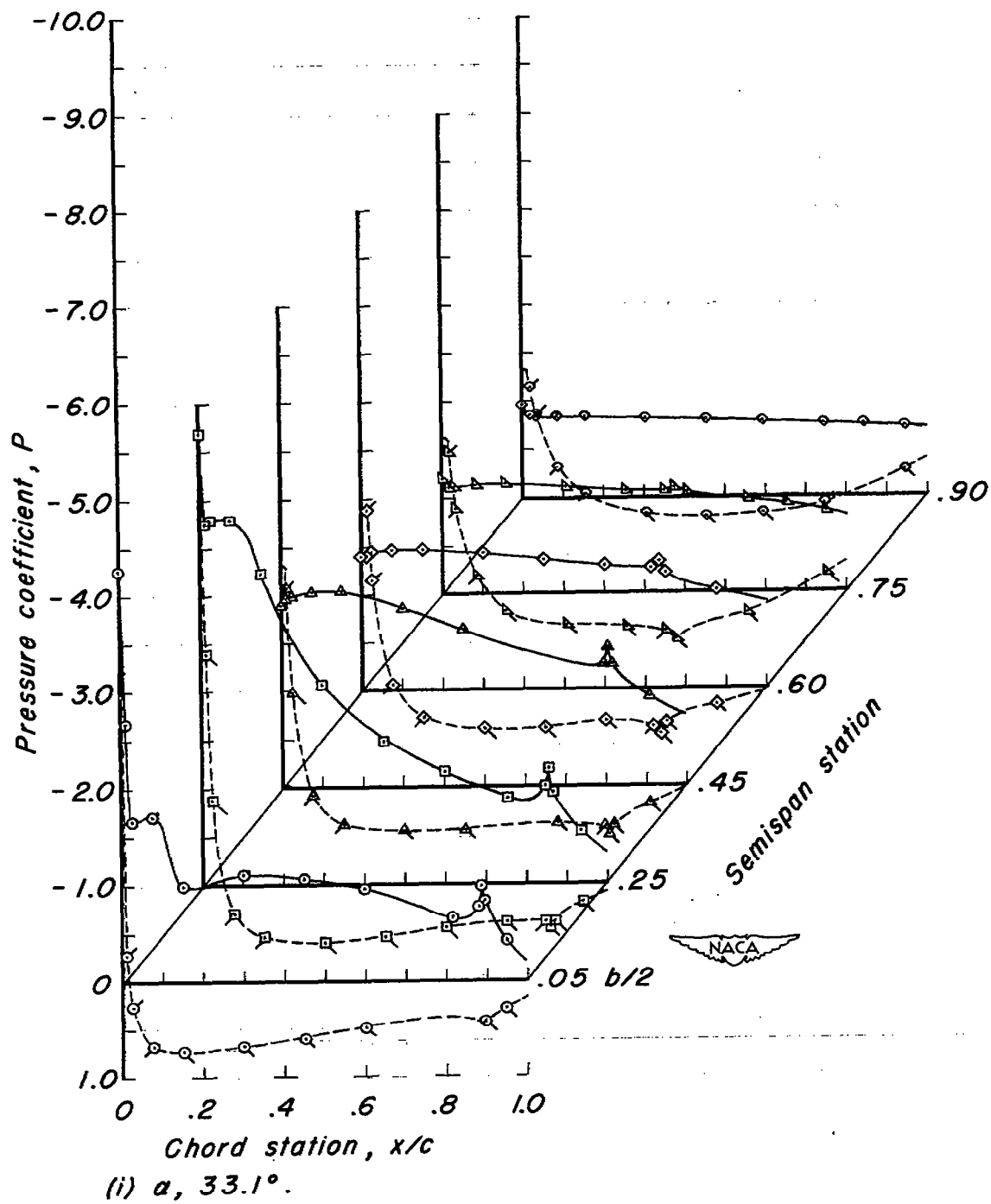
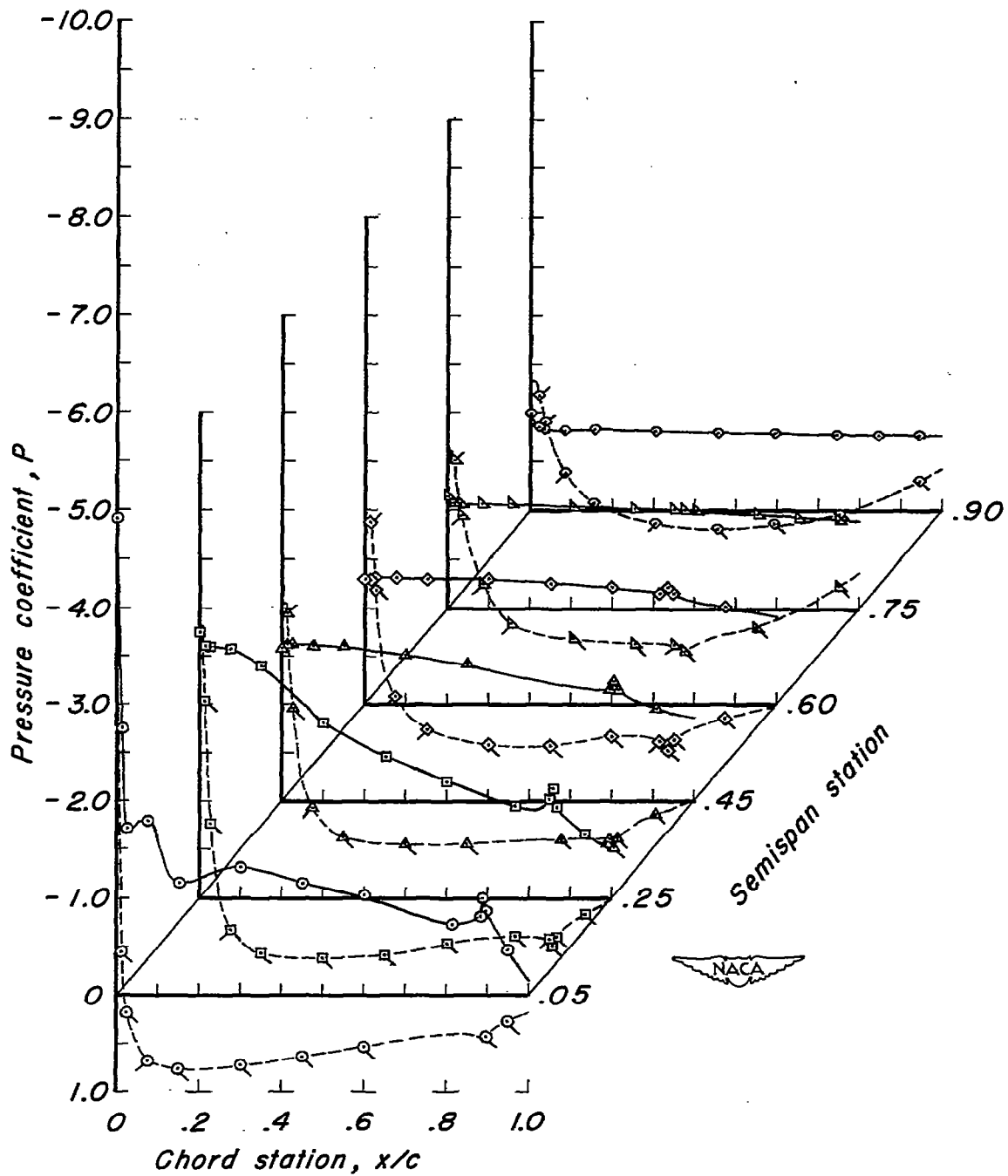


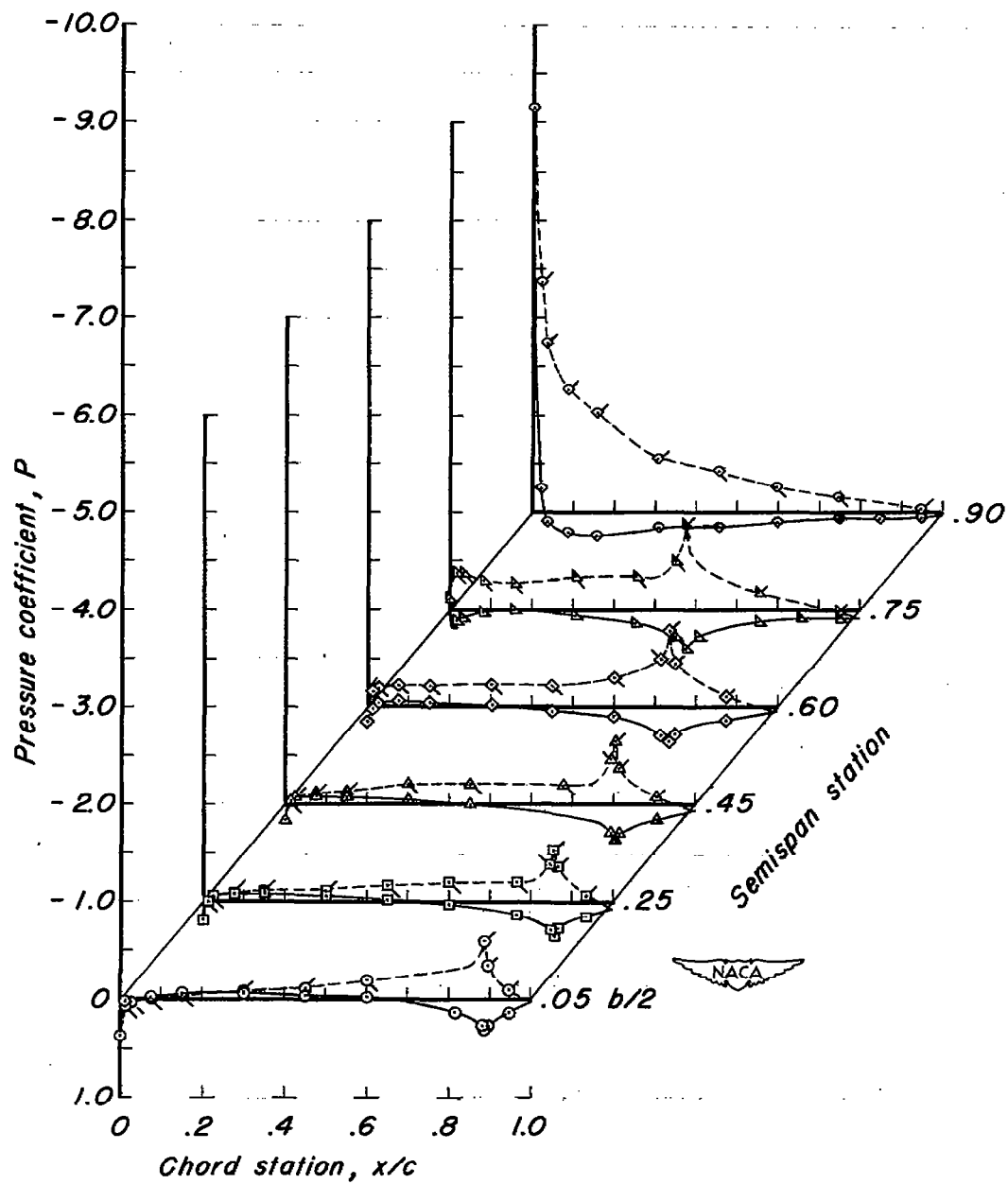
Figure 6.- Continued.



(j) $\alpha, 37.0^\circ$.

Figure 6.- Concluded.

Flagged symbols and dashed curves indicate lower surface pressures.



(a) $\alpha, -0.1^\circ$.

Figure 7.— Pressure distribution along chord for various angles of attack. $\delta_{f_n}, -10^\circ$.

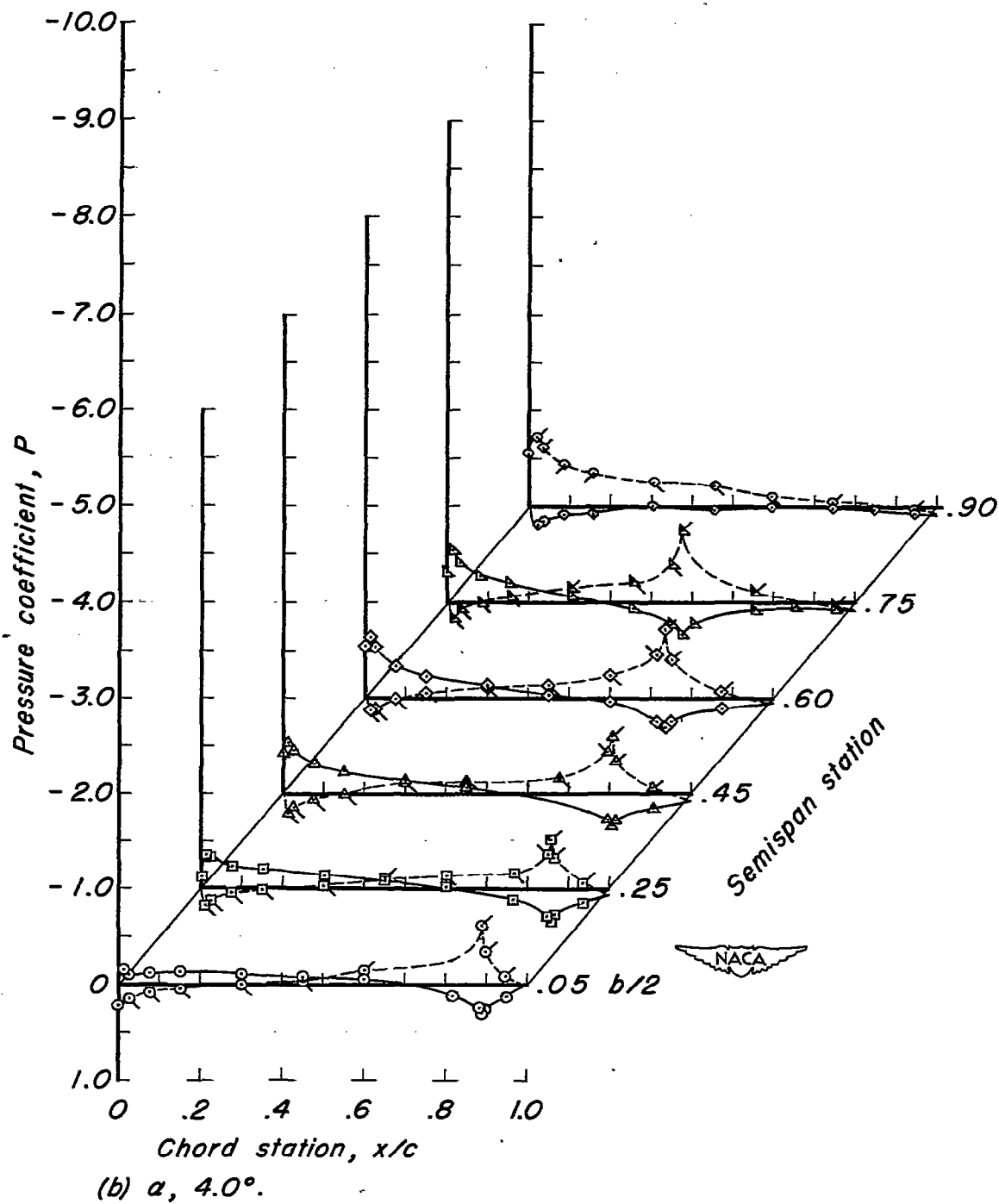


Figure 7.- Continued.

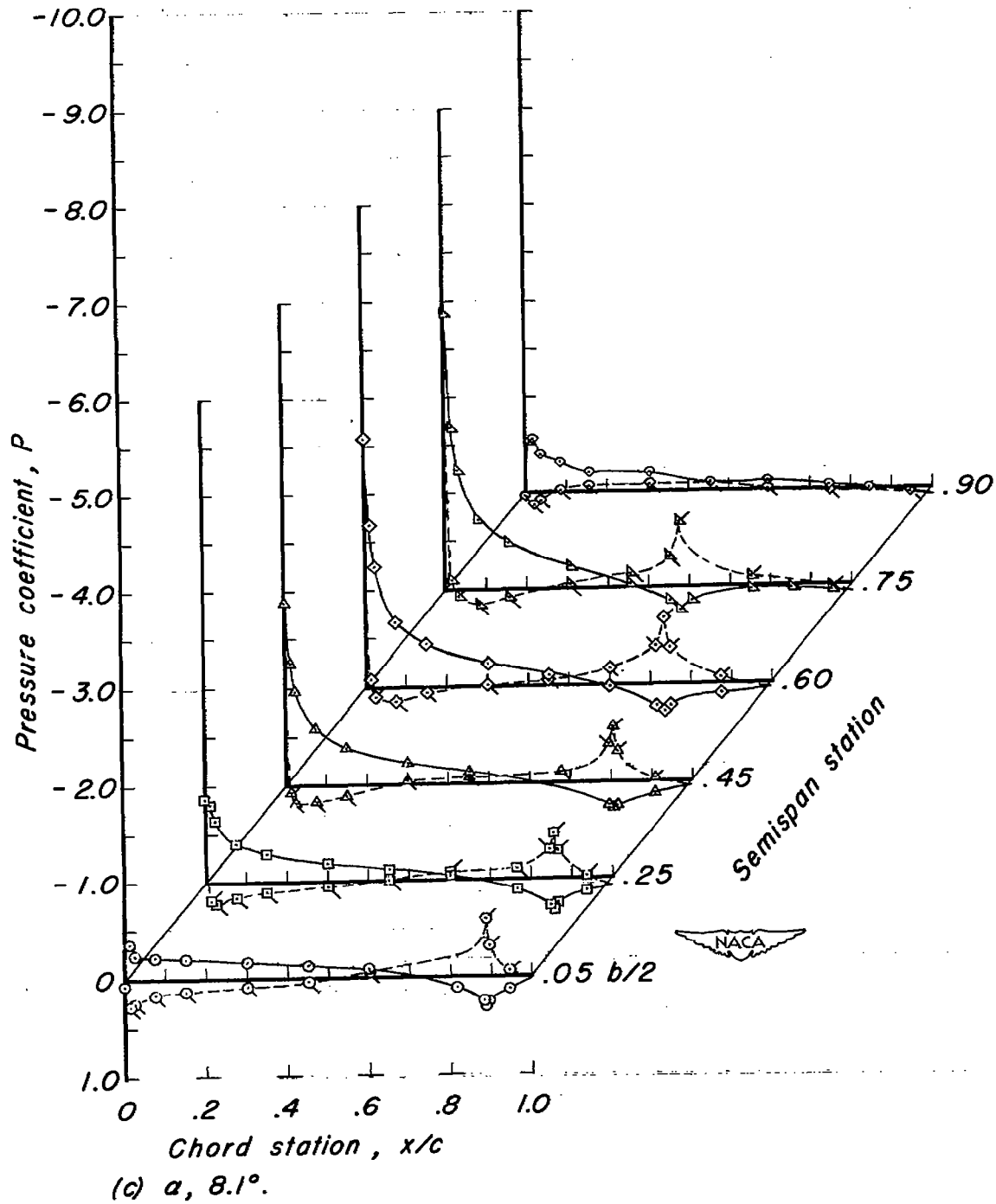


Figure 7.- Continued.

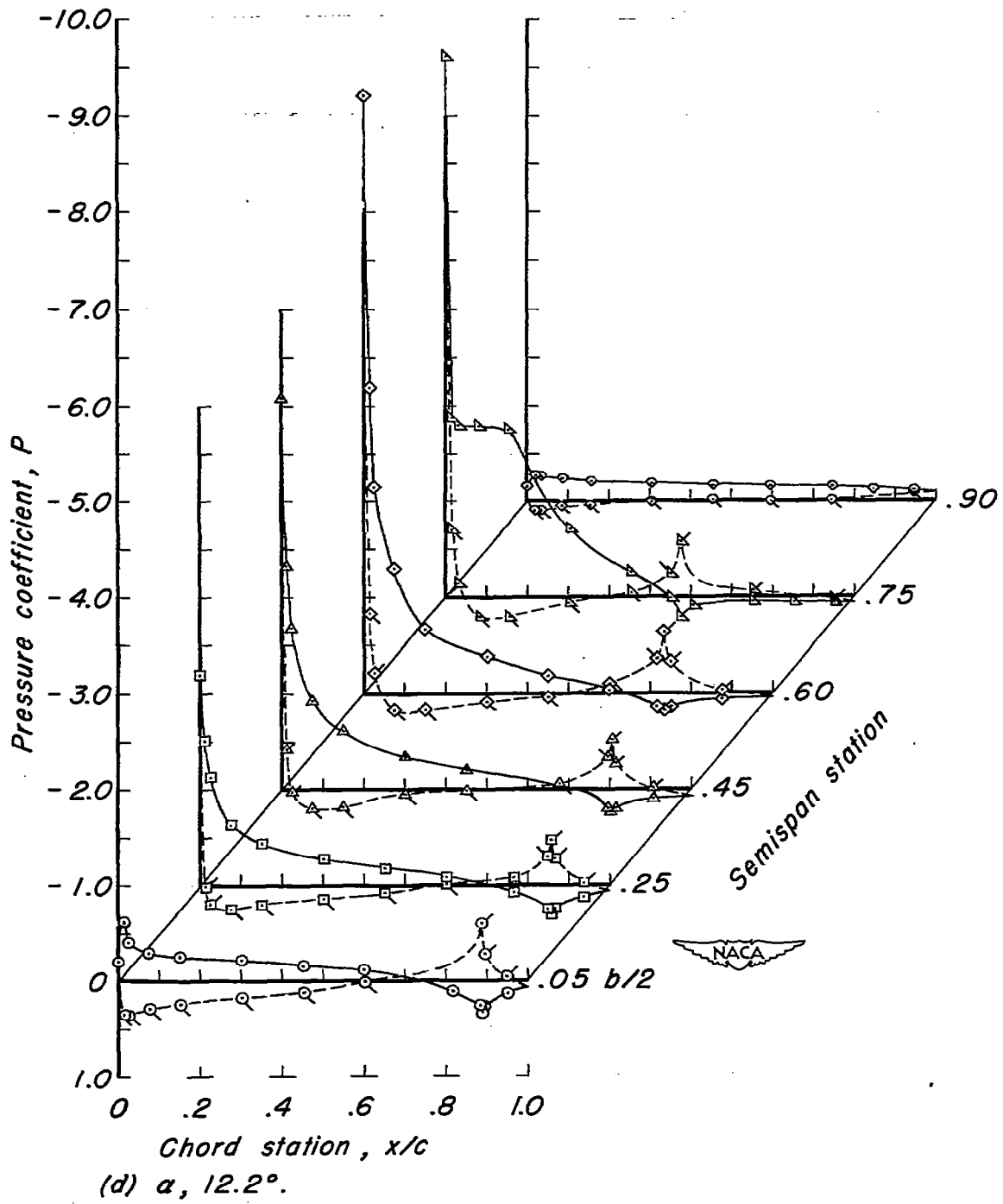


Figure 7.- Continued.

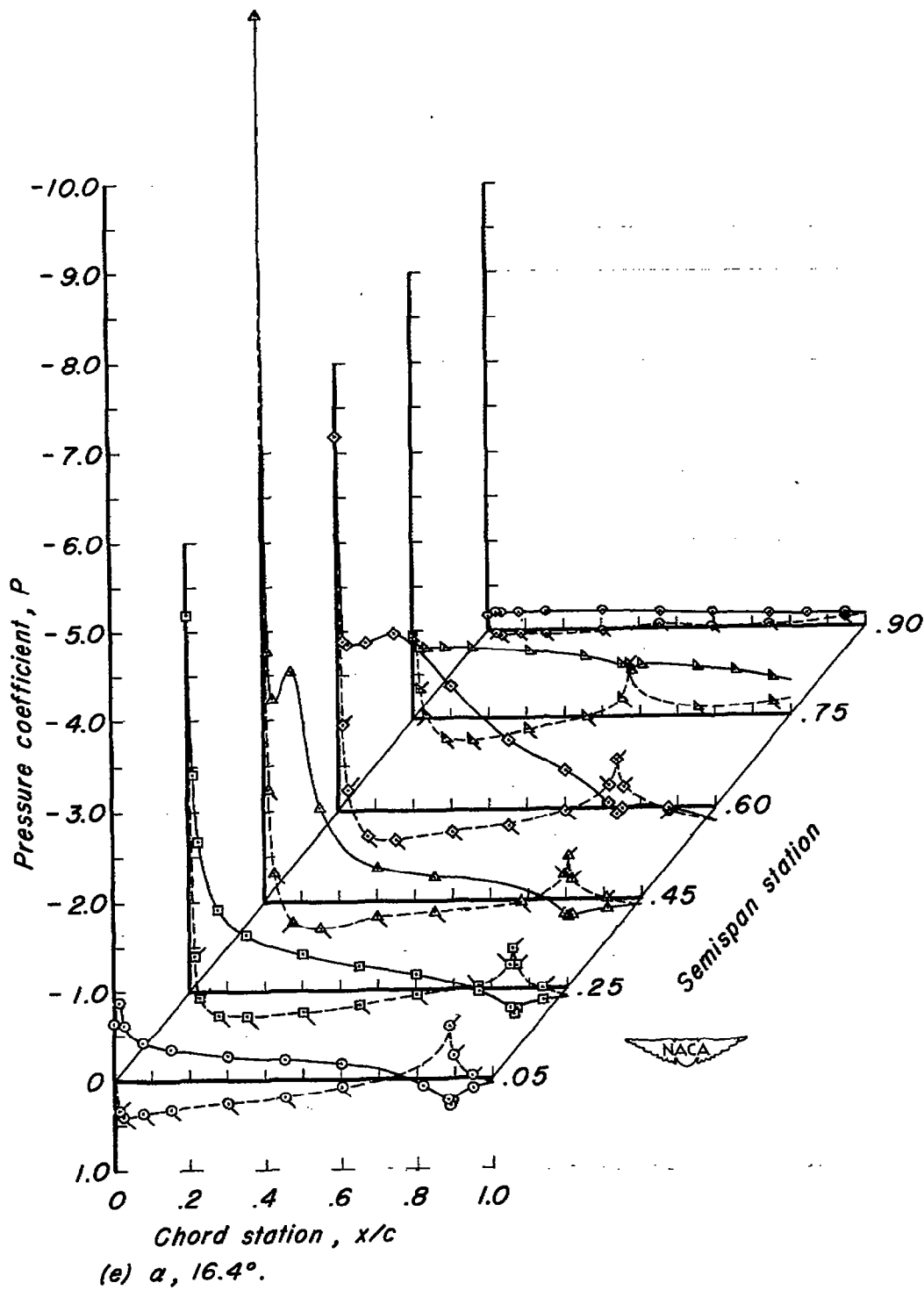


Figure 7.- Continued.

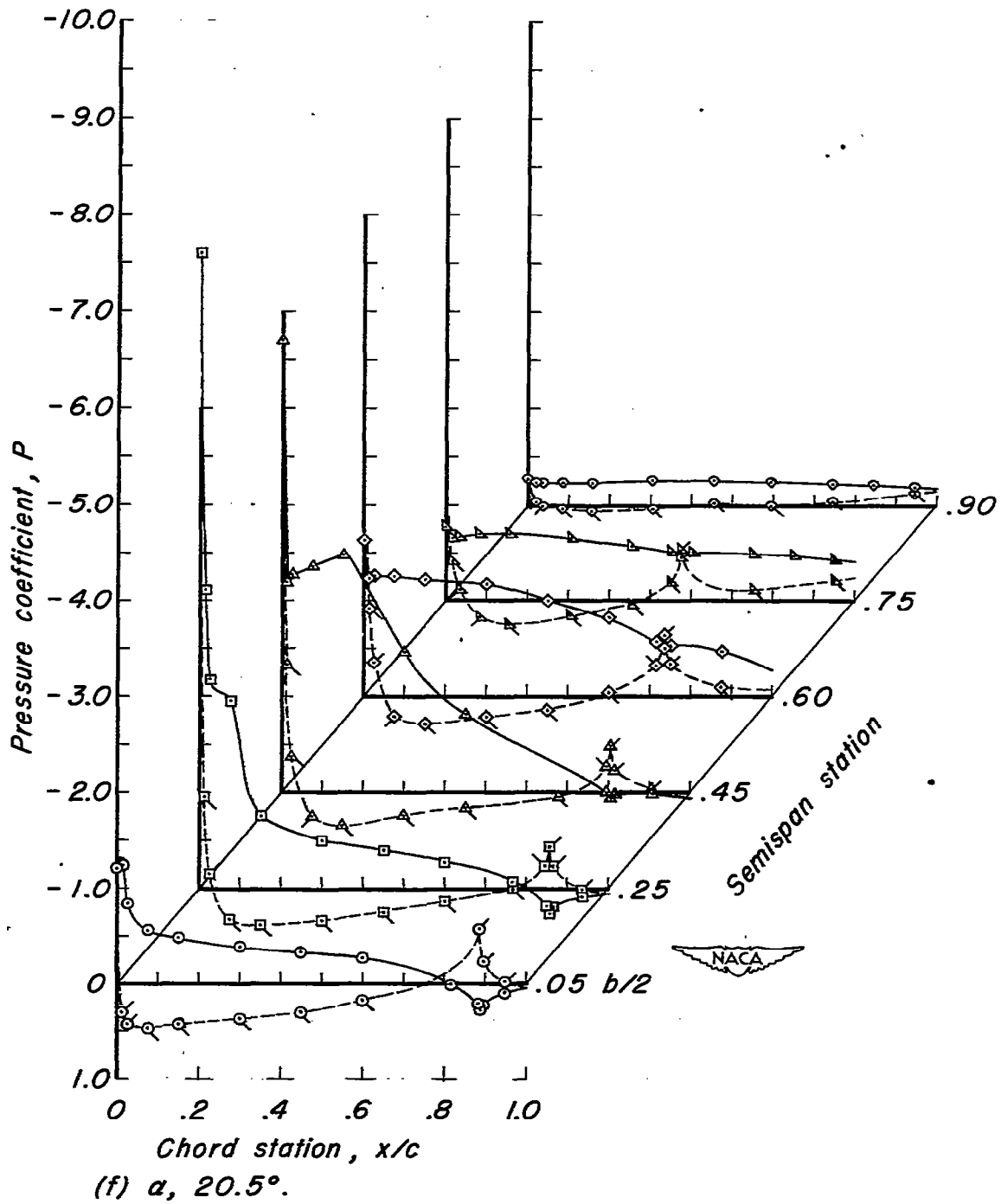


Figure 7.- Continued.

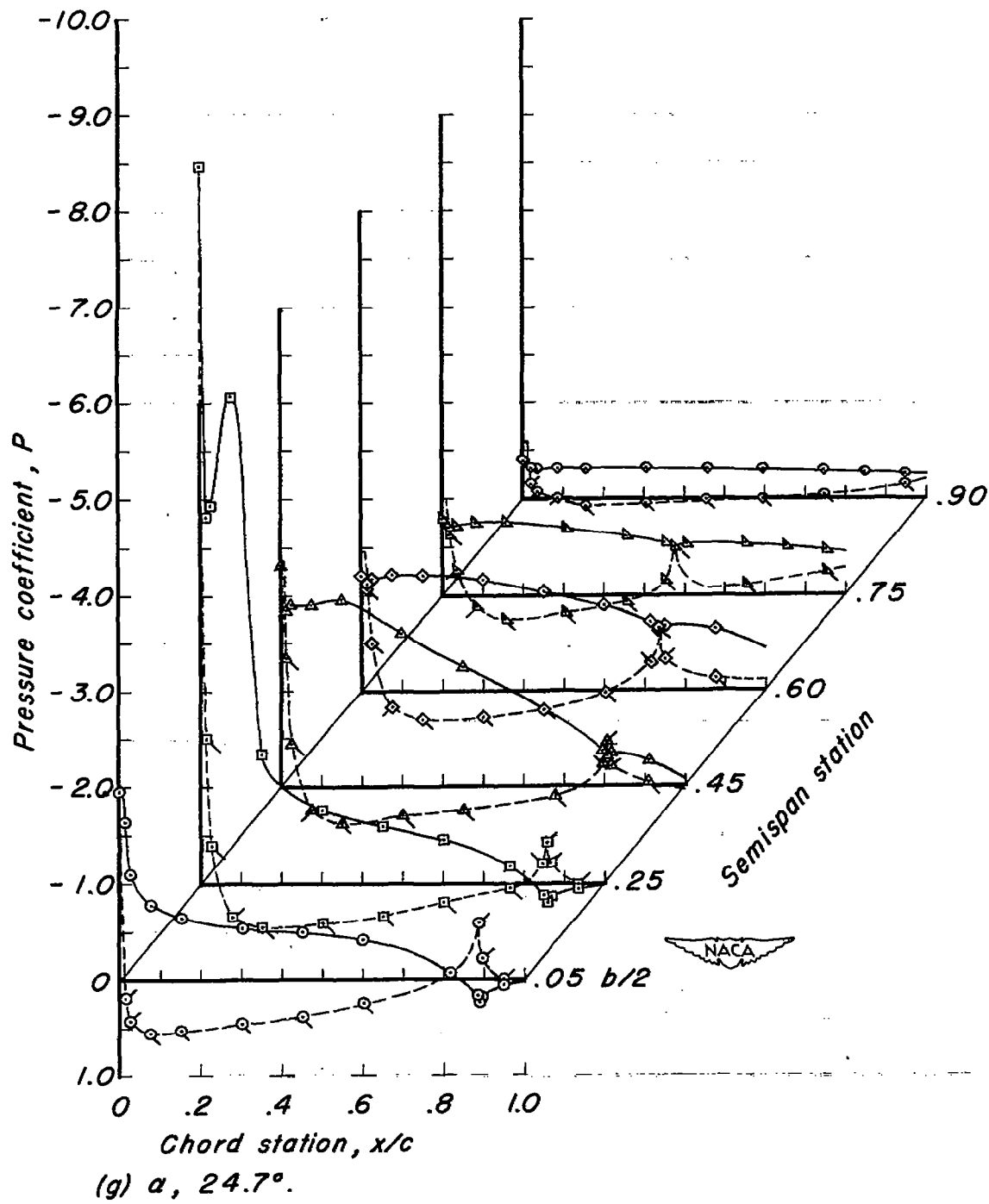


Figure 7.-Continued.

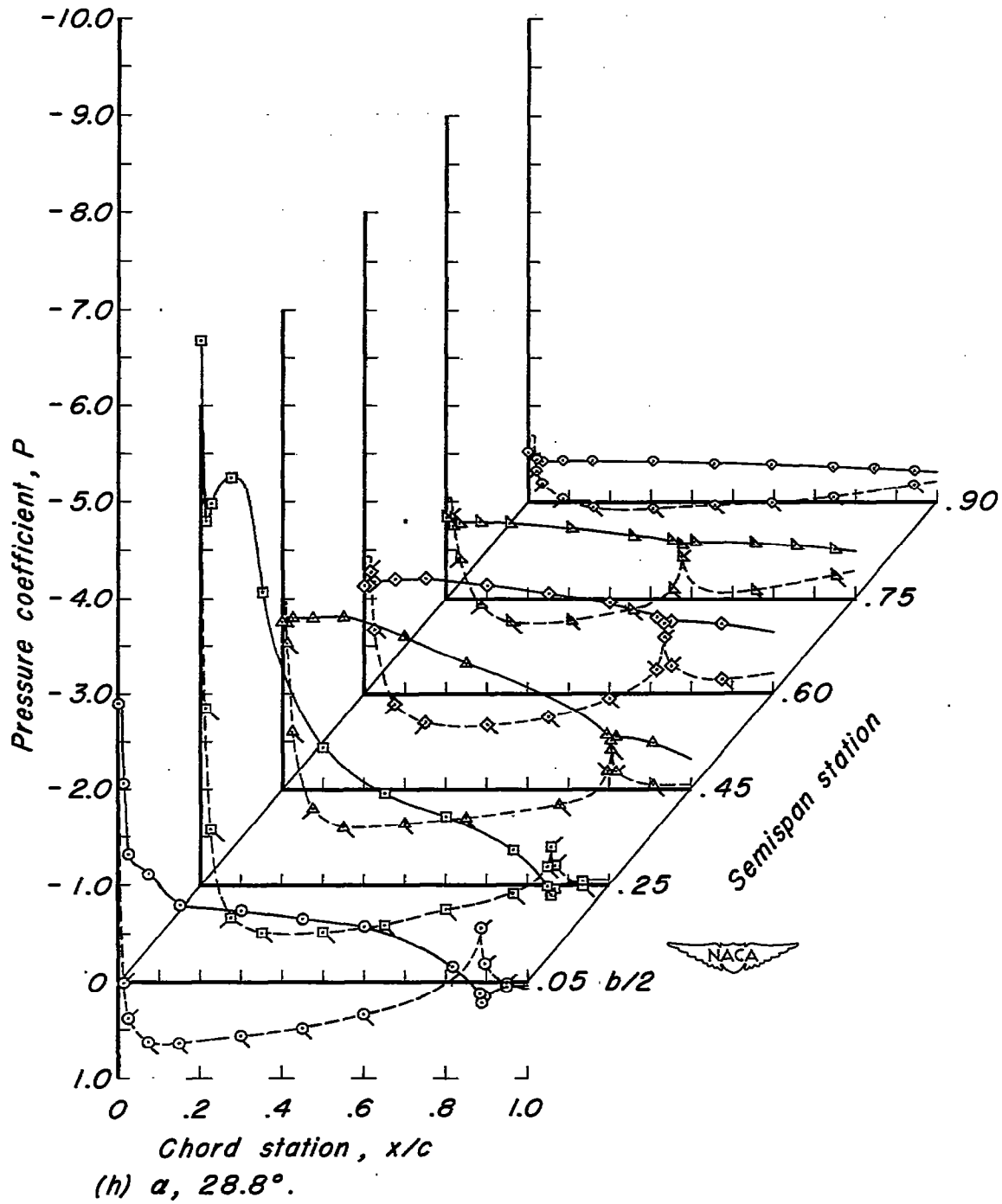
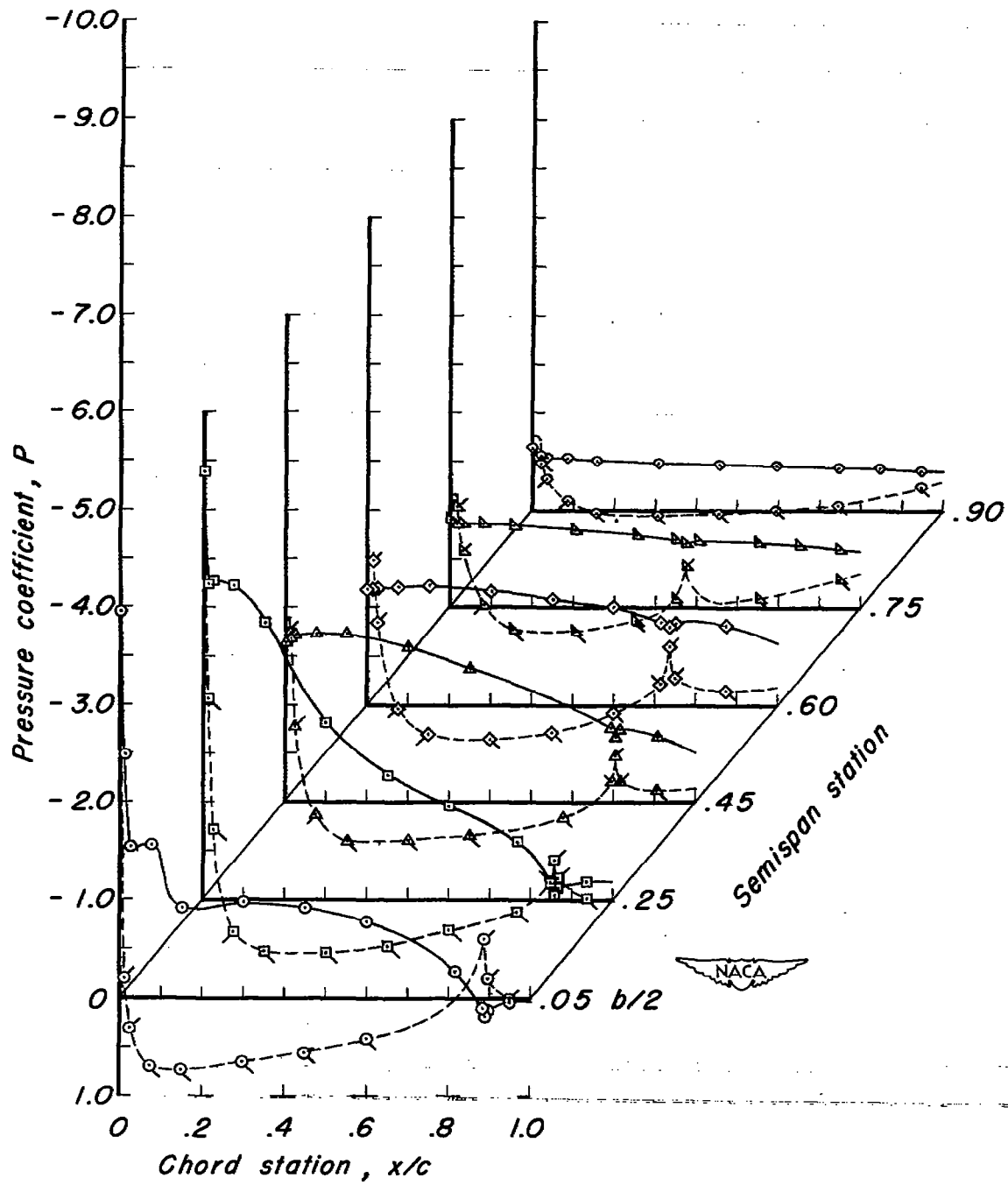


Figure 7.- Continued.



(i) α , 32.9° .

Figure 7.- Continued.

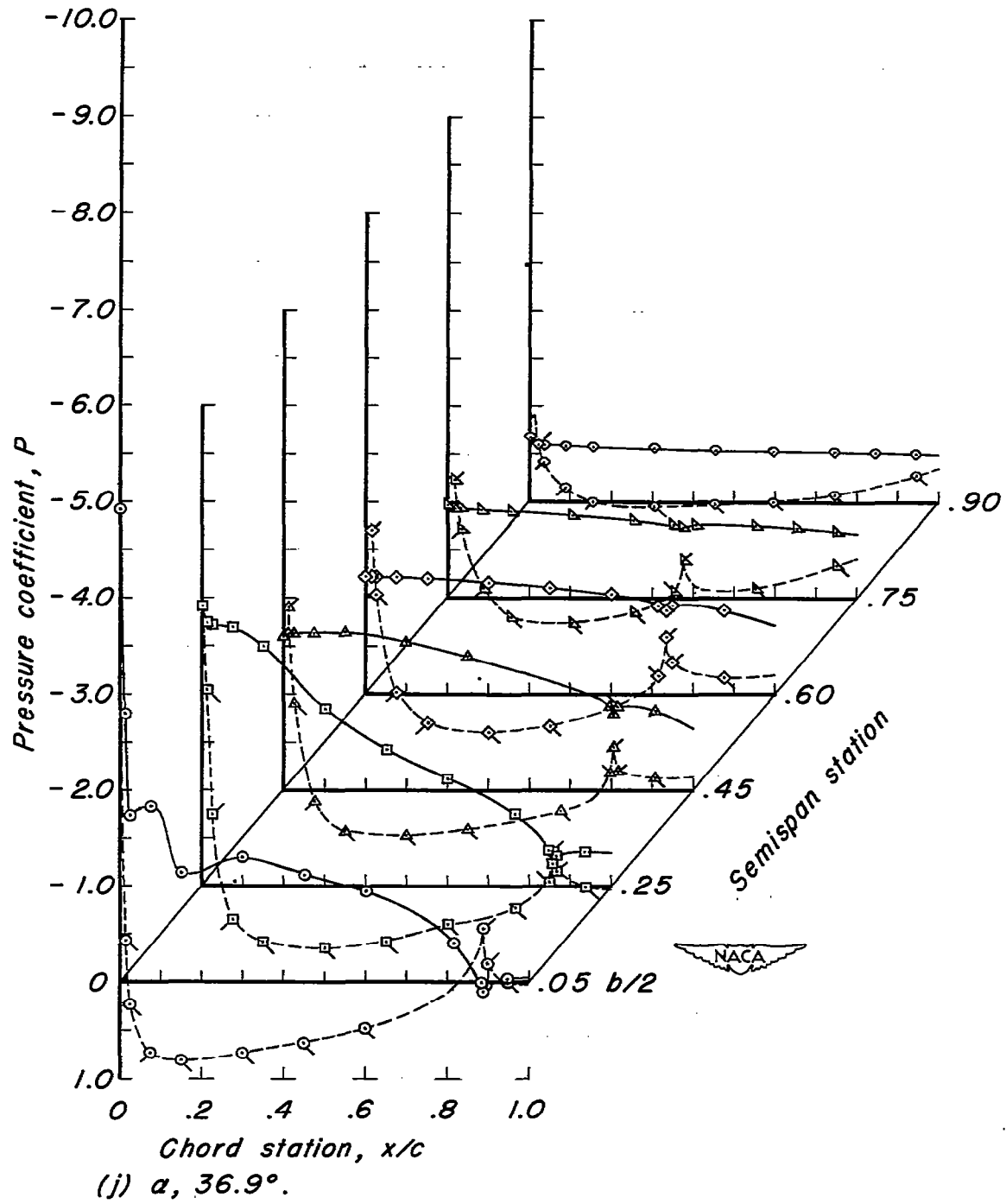


Figure 7.- Concluded.

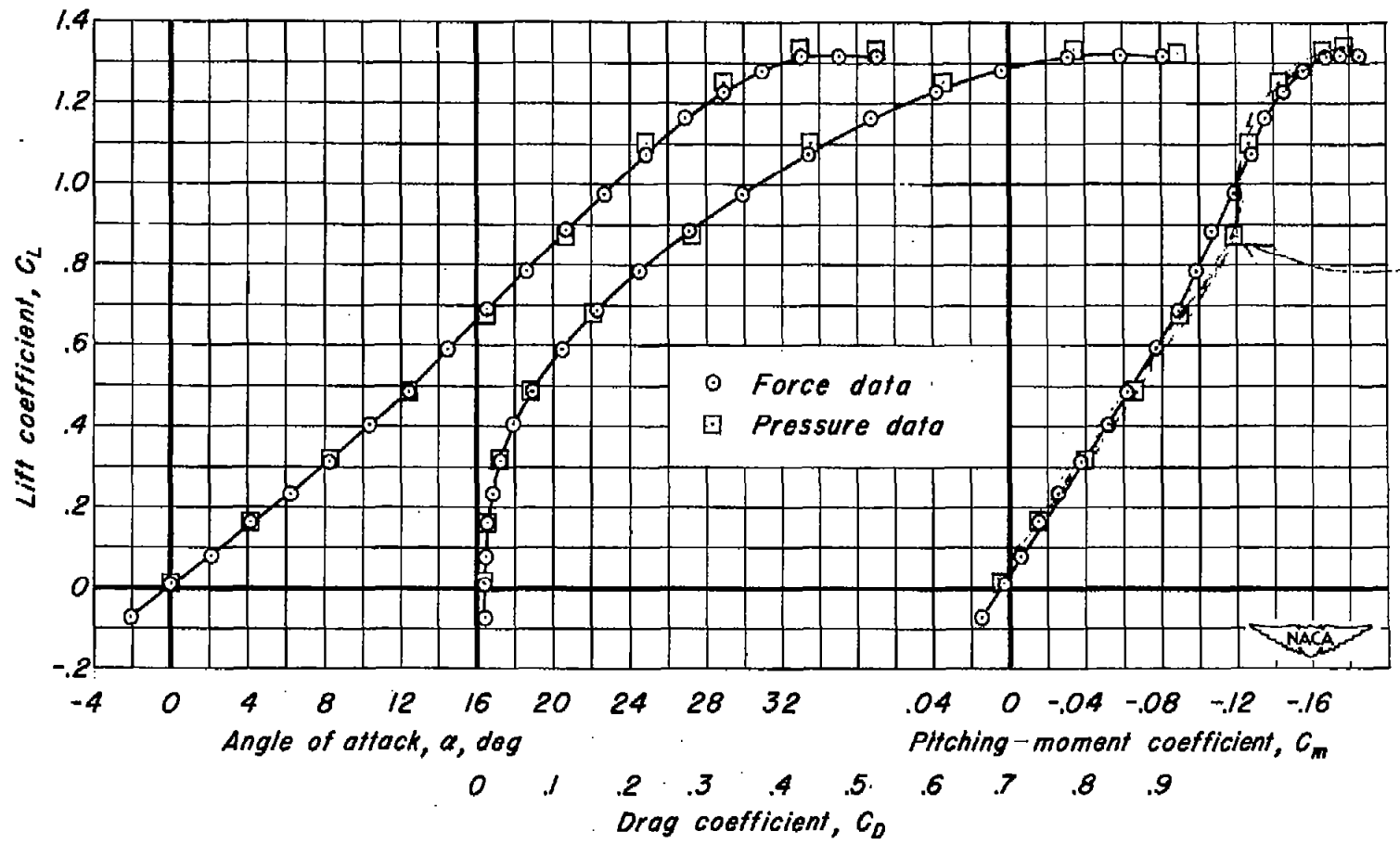
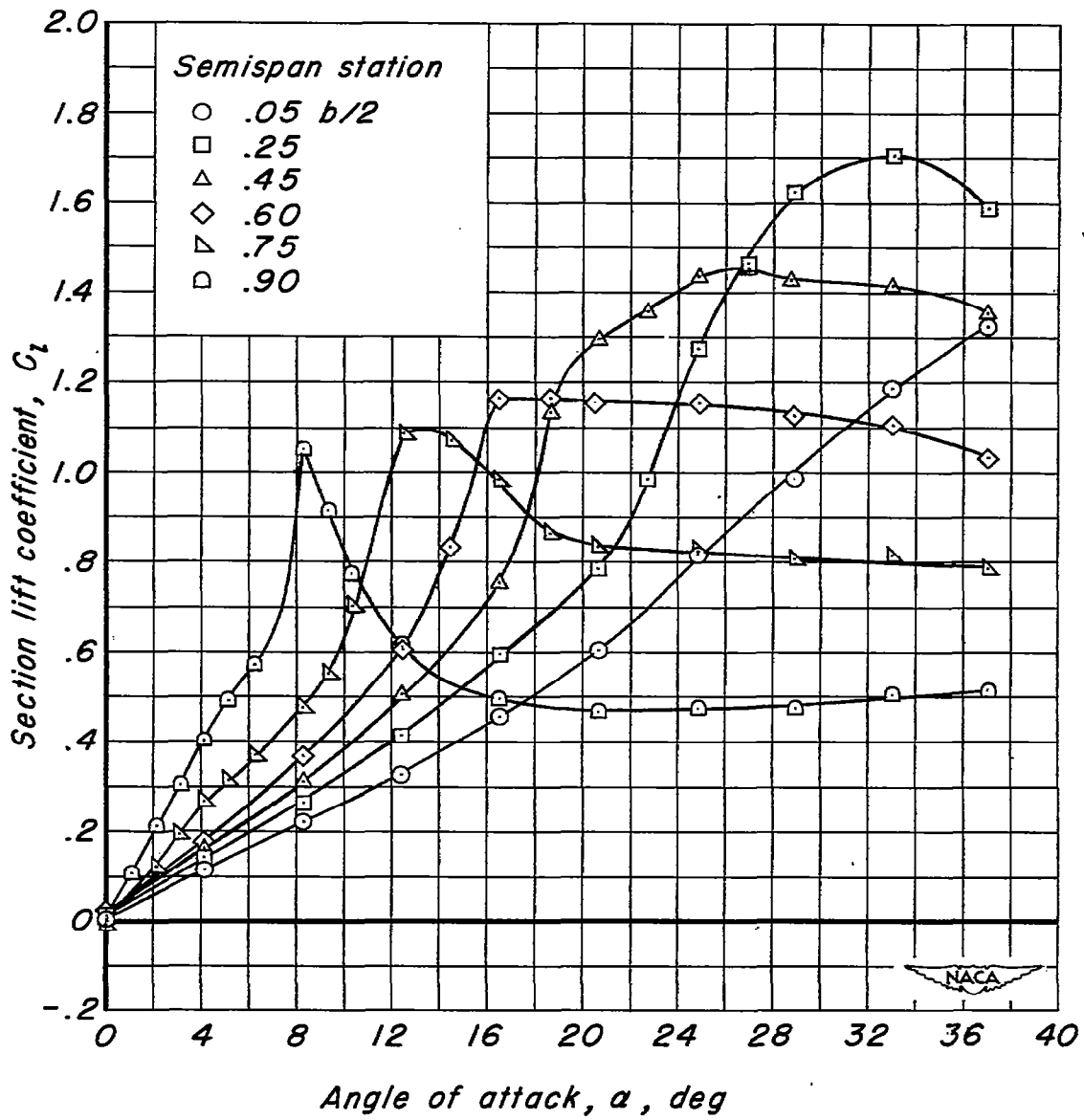
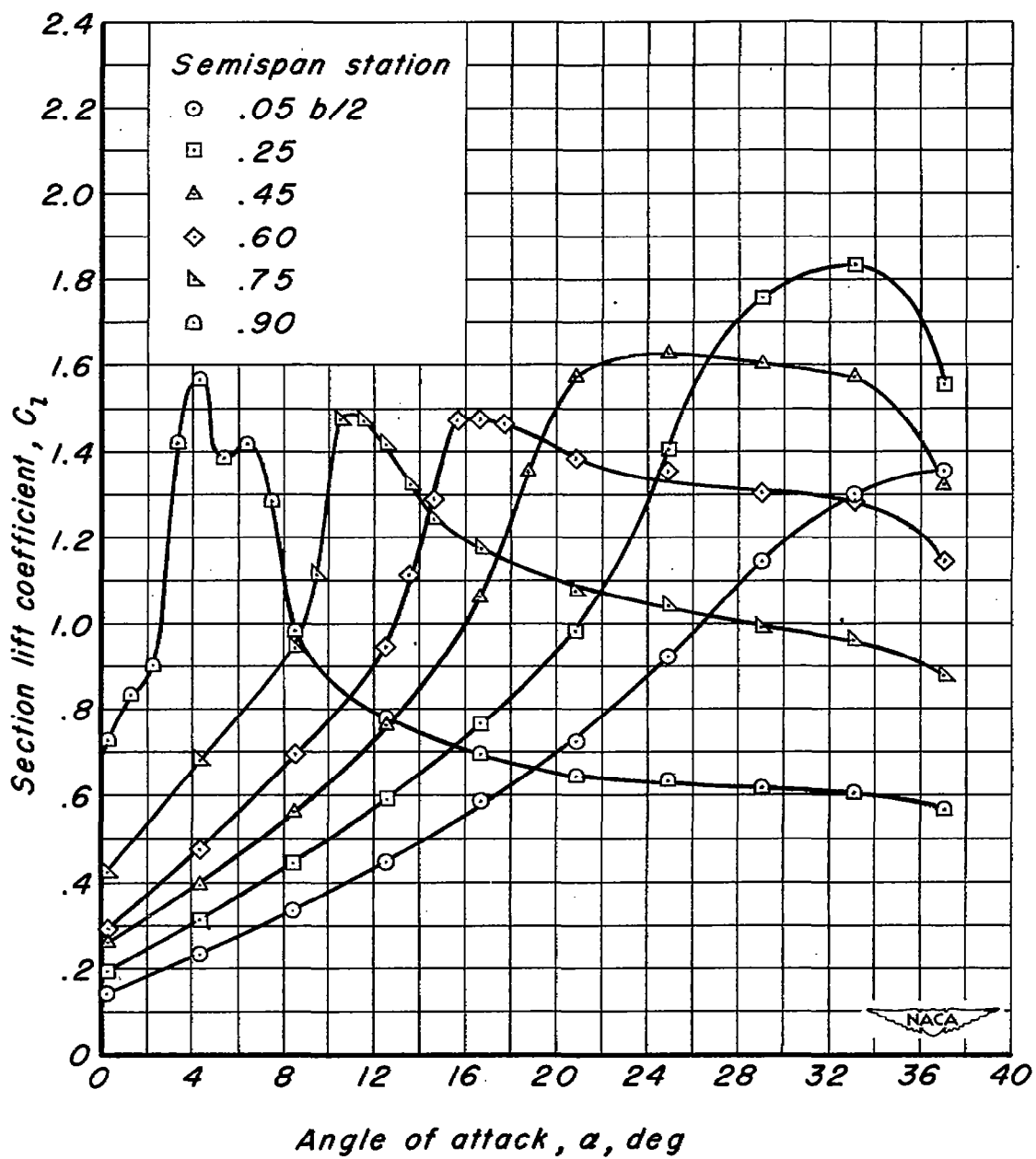


Figure 8.- Comparison of aerodynamic characteristics obtained from force-test data and from integration of pressure data.



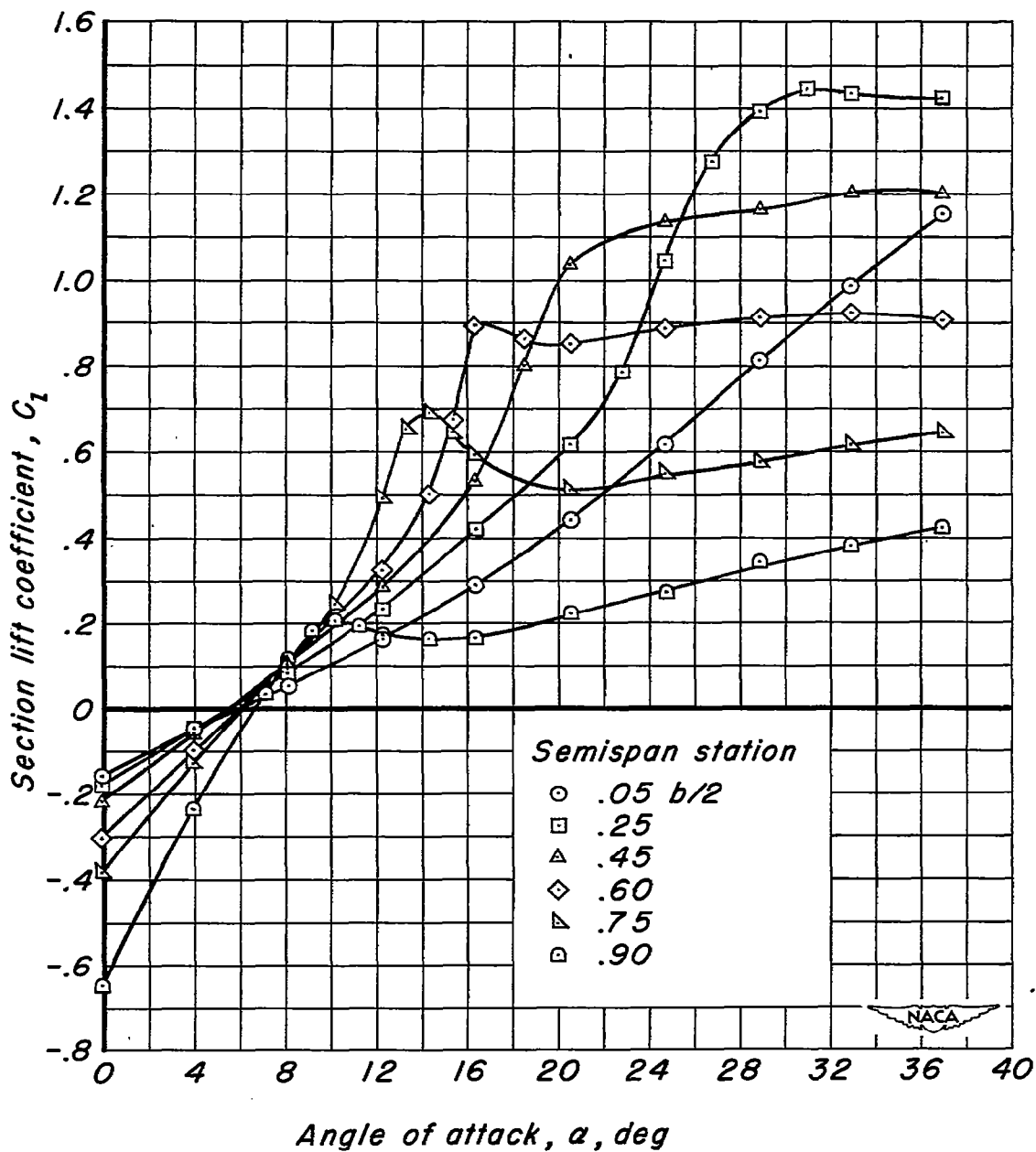
(a) $\delta_{f_n}, 0^\circ$.

Figure 9.- Section lift curves for several spanwise wing stations.



(b) $\delta_{fn}, 10^\circ$.

Figure 9.- Continued.



(c) $\delta_{f_n}, -10^\circ$.

Figure 9.- Concluded.

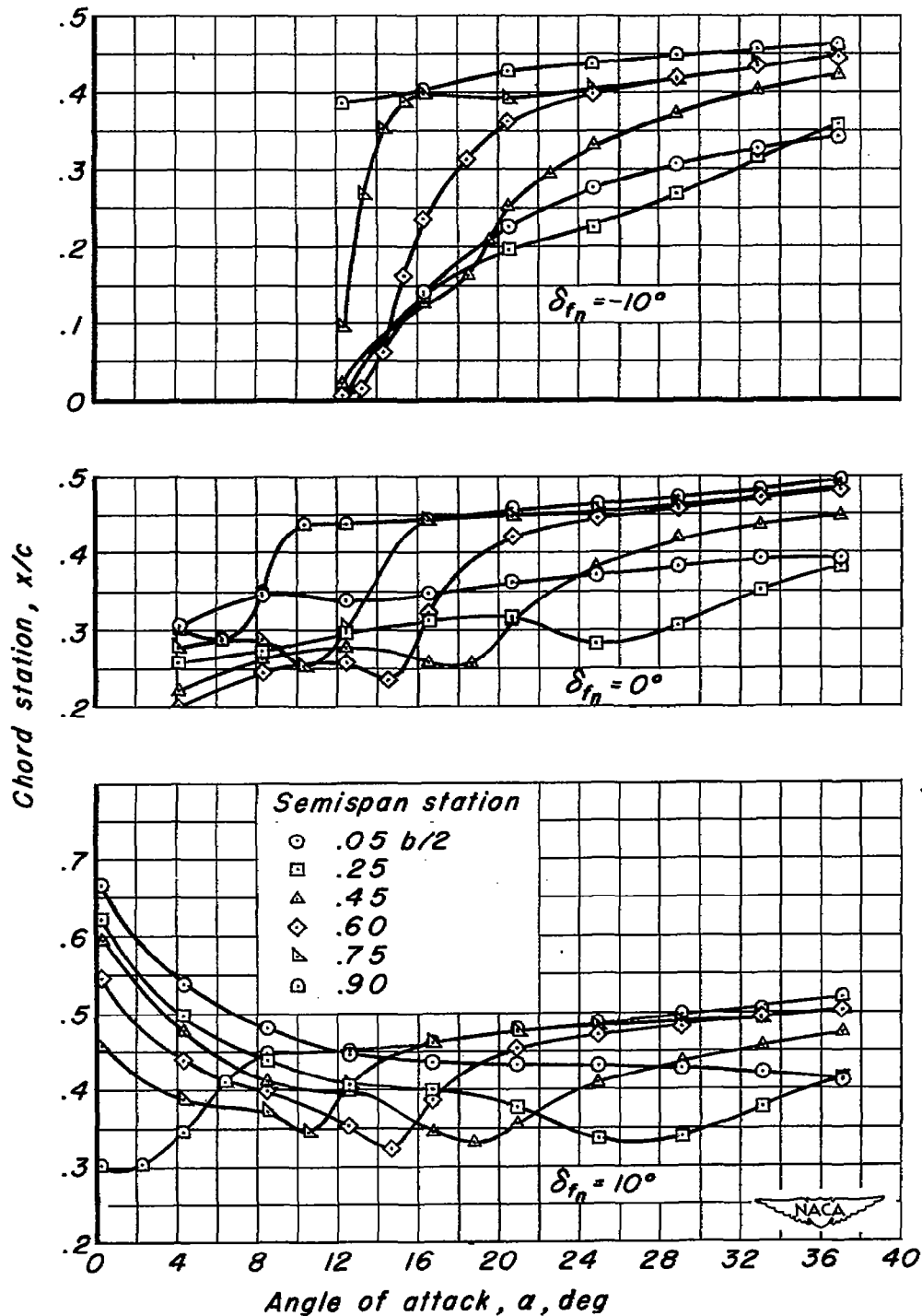
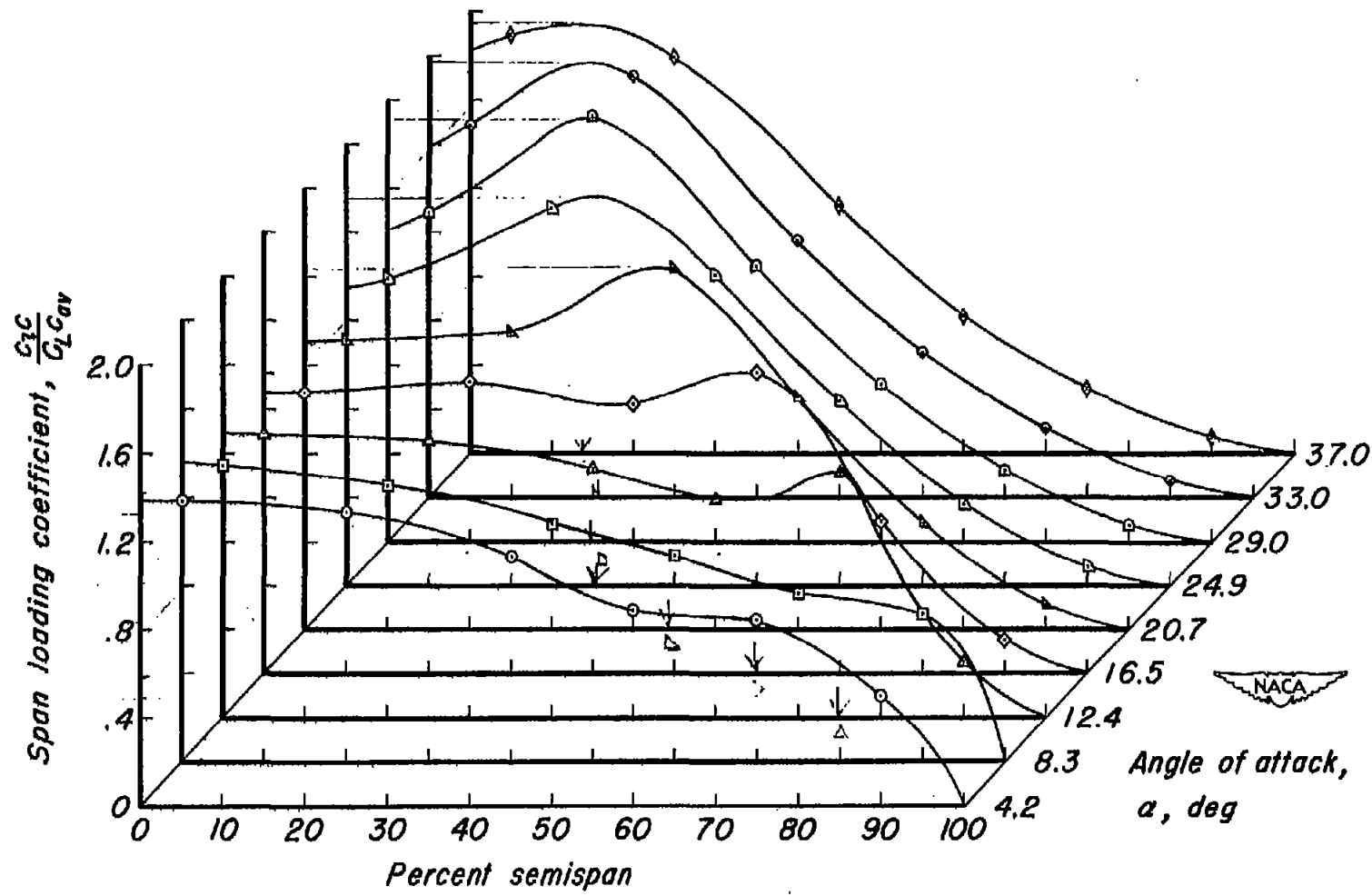
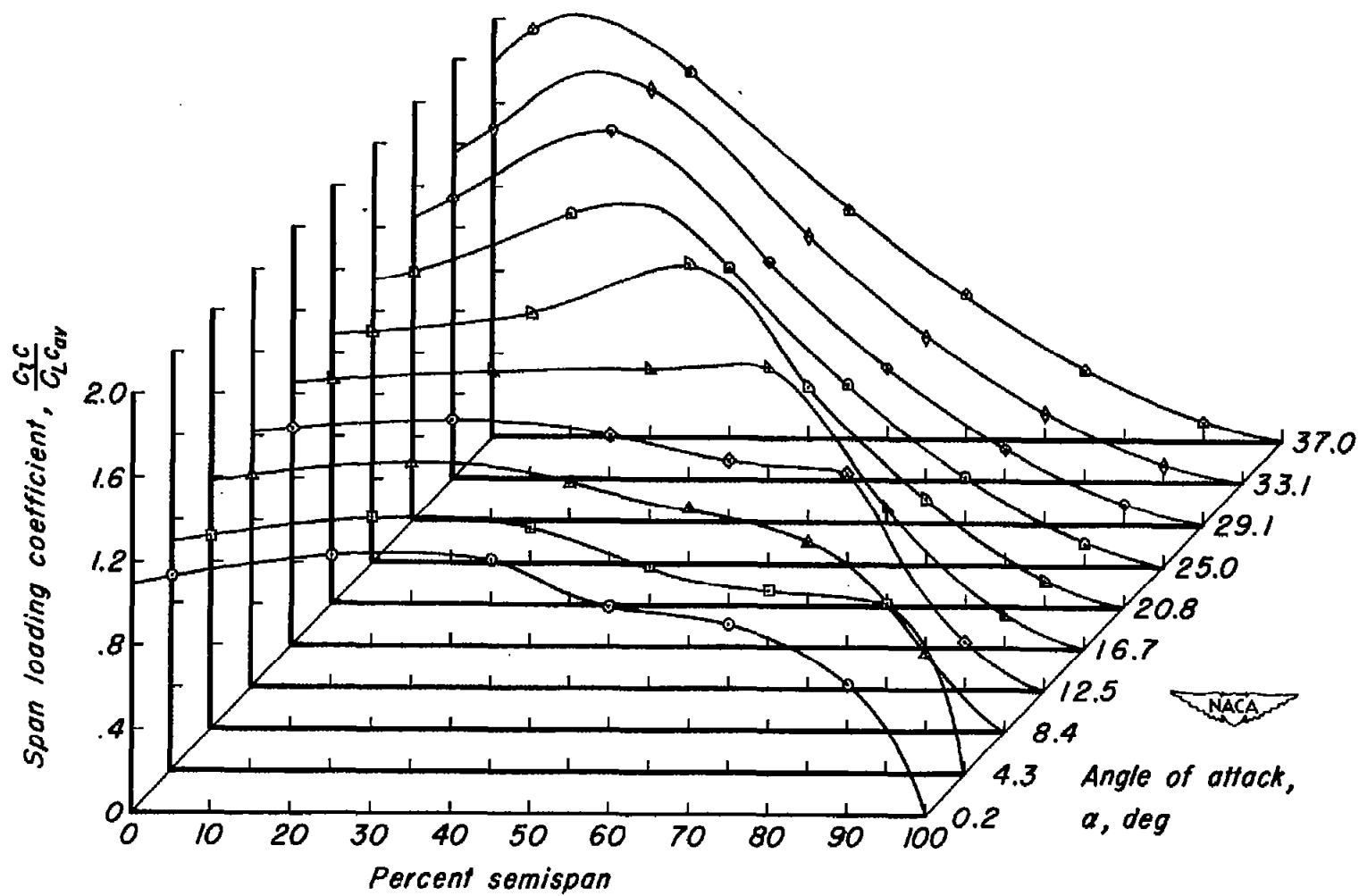


Figure 10.- Variation of chordwise center of pressure for several spanwise wing stations.



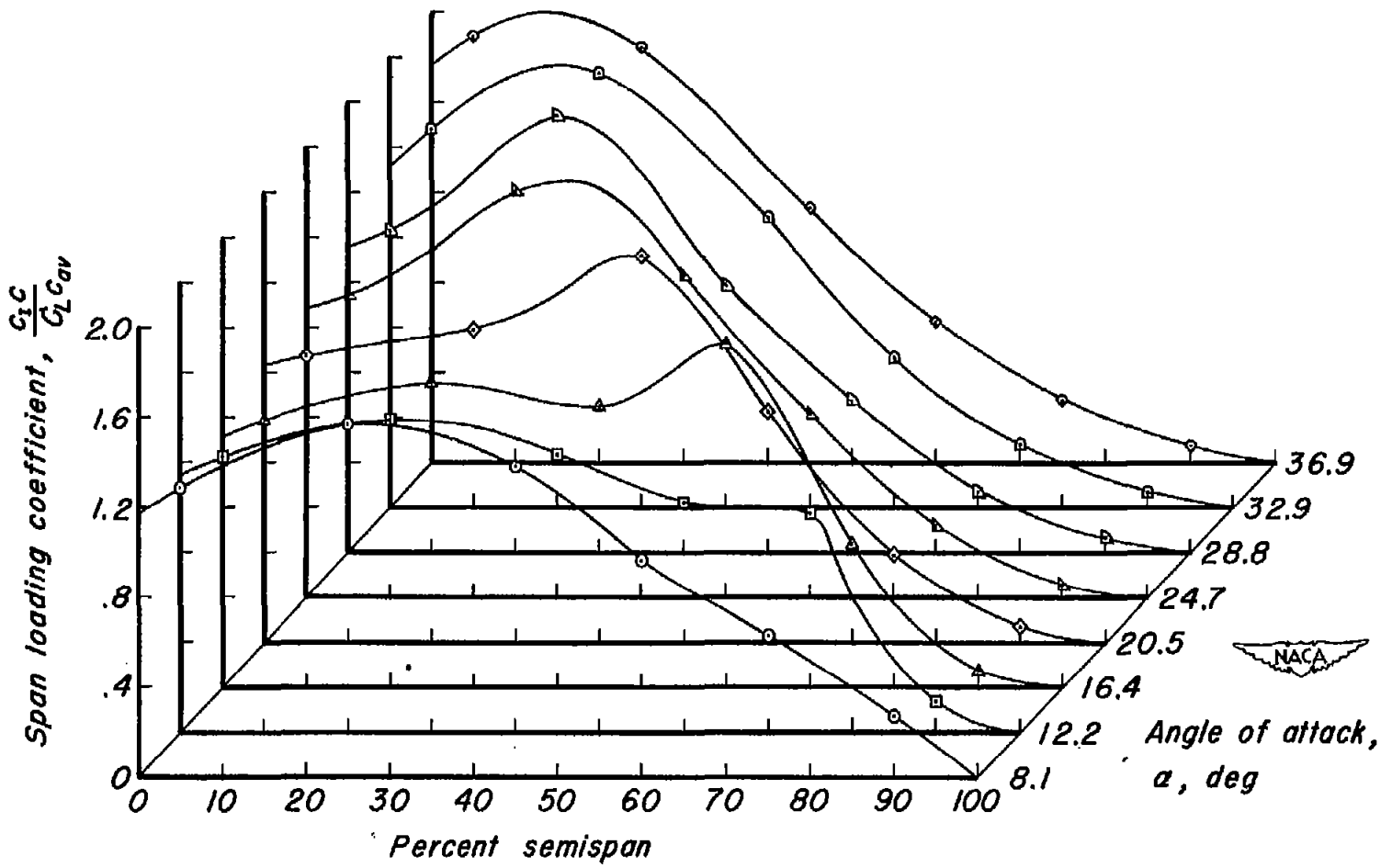
(a) $\delta_{fn}, 0^\circ$.

Figure 11.- Span load distribution for several angles of attack.



(b) $\delta_{t_n}, 10^\circ$.

Figure 11.- Continued.



(c) $\delta_{fn}, -10^\circ$.

Figure 11.- Concluded.